Fachhochschule Hamburg
Fachbereich
Naturwissenschaftliche Technik

Alignment of Transmission Electron Microscopy Images Acquired During a Tilt Series by Tracking Fiducial Markers

Diplomarbeit

im Studiengang Medizintechnik

vorgelegt von
Kerstin Stockmeier
aus
Ludwigshafen am Rhein

10. November 2000

Gutachter:
Prof. Dr. Manfred Herbst, FH Hamburg
Dr. Thomas Köhler, Philips GmbH Forschungslaboratorien, Hamburg

Contents

1 Introduction **1**

2 Theoretical Background **3**

2.1 Transmission Electron Microscopy 3

2.2 Electron Tomography 11

2.3 Image Registration 13

2.4 Methods for Automatic Alignment 14

3 Materials and Methods **16**

3.1 Phantom Data 16

3.2 Real Data 16

3.3 Misalignment Estimation by Cross-Correlation 17

3.3.1 Equalization of the Geometric Properties of Projections by Cosine Stretching 19

3.4 Detection of Fiducial Markers 19

3.5 Marker Indexing 22

3.5.1 Hough Transform 23

3.5.2 Determination of Regions of Interest 25

3.5.3 Marker Tracing Based on the Hough Transform 29

4 Results **35**

4.1 Simulations 35

4.2 Selection of Later Traced Markers 35

4.3 Tracing of Markers 38

4.3.1 Reasons for the Failure of the Prediction 41
4.3.2 Indexing Quality 42
4.4 Overlapping of Detected Marker Chains 43

5 Discussion **46**

6 Summary **49**

7 References **50**

A Mathematical fundamentals **53**
A.1 The Fast Fourier Transform 53
A.2 The Cross-Correlation Function 54

B Marker tracing **55**

Chapter 1

Introduction

With electron tomography the 3D structure of an object can be obtained by reconstructing from a tilt series of 2D projection. This method has been beneficial in biologic research as a high volumetric resolution can be achieved. It is used for the characterization of macromolecules, viruses, and cellular organelles in in-vitro preparations [HA96][MBF+95][Rad88][ZPJ+94].
One of the limiting factors of the image quality obtained by the reconstruction is the precision of alignment of the projections [FM92]. There are different approaches to resolve the alignment step. One approach is to deposit fiducial markers during the specimen preparation to get easy identifiable high-contrast regions. At the present time, the acquisition of these markers often involves operator interaction. This process results in appropriate accuracy but is tedious and time-consuming should numerous tilt images come into register. In addition, operator based identification of markers is a subjective process and requires extensive experience to get a satisfactory result [RHS+99]. An automatic alignment is commonly done with cross-correlation [FM92]. But this does not always result in a satisfactory accuracy.
In the following thesis, an alignment method combining cross-correlation with the tracking of fiducial markers is described in detail. It can be broken down into three steps: Preprocessing the images with cross-correlation, detection

of fiducial markers with a pattern recognition algorithm, and establishment of overlapping chains of indexed markers throughout the tilt series.
This thesis is structured as follows: In chapter two some background information is given on the principles of transmission electron microscopy, basic ideas of 3D electron microscopy and on state of the art aligning 2D projections using fiducial markers. Chapter three consists of a description of the image data used and a specification of the registration algorithm. Chapter four summarizes the results obtained with simulated data and real data, and includes a description of the traceability of the fiducial markers. Chapter five consists of a discussion and concludes with a brief summary of the perspectives for this method.

Chapter 2

Theoretical Background

2.1 Transmission Electron Microscopy

The Transmission Electron Microscope (TEM) is similar to a slide projector which is illustrated in Fig. 2.1. There, emitted light is parallelized by a condenser lens. The light beam passes the slide (object) and is focused on a screen by an objective lens. In TEM the light source is replaced by an electron source. The optical lenses are substituted by magnetic lenses as well as the screen is substituted by a fluorescent screen that emits light when electrons hit it. The passage from the electron source to the fluorescent screen is evacuated since the mean free path of electrons in air is very small. The object has to be prepared extremely thin to ensure that electrons are able to pass it: biological specimen are normally prepared in the order of some 100 nm thickness. In addition the TEM provides a high spatial resolution (<1nm), which is described in more detail later in this chapter.

Effects of the Electron Beam

As the electron beam travels through the sample, scattering processes take place. Mainly two types of scattering processes can be distinguished:

- elastic scattering, which is the interaction of the beam electrons and the potential field around the nuclei and involves no energy loss, and

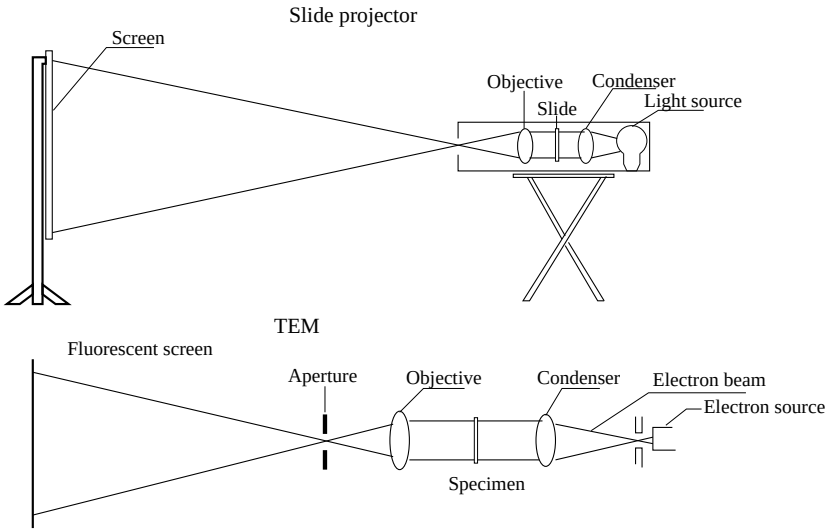

Figure 2.1: The TEM in comparison with a slide projector. [phi]

- inelastic scattering, which is the interaction of the beam electrons with the electrons of the sample and involves energy losses and absorption.

Fig. 2.2 shows the electromagnetic waves and electrons emitted by the specimen as a result of the scattering processes. In the following the particular processes are briefly reviewed.

1. Some electrons are absorbed by the specimen and scattering processes modify the beam's intensity. This effect is dependent on the specimen's density and its chemical composition (amplitude contrast).

2. Considering the electron beam as a wave, the interaction of the specimen with the beam results in shifts in the relative phases of the portions of the beam contributing to the image (phase contrast).

3. In crystalline samples the elastic scattering is coherent and results in spot patterns (Bragg diffraction).

4. Some electrons are reflected by the specimen (backscattered electrons).

5. Electrons hitting the specimen may cause emission of electrons (secondary electrons).

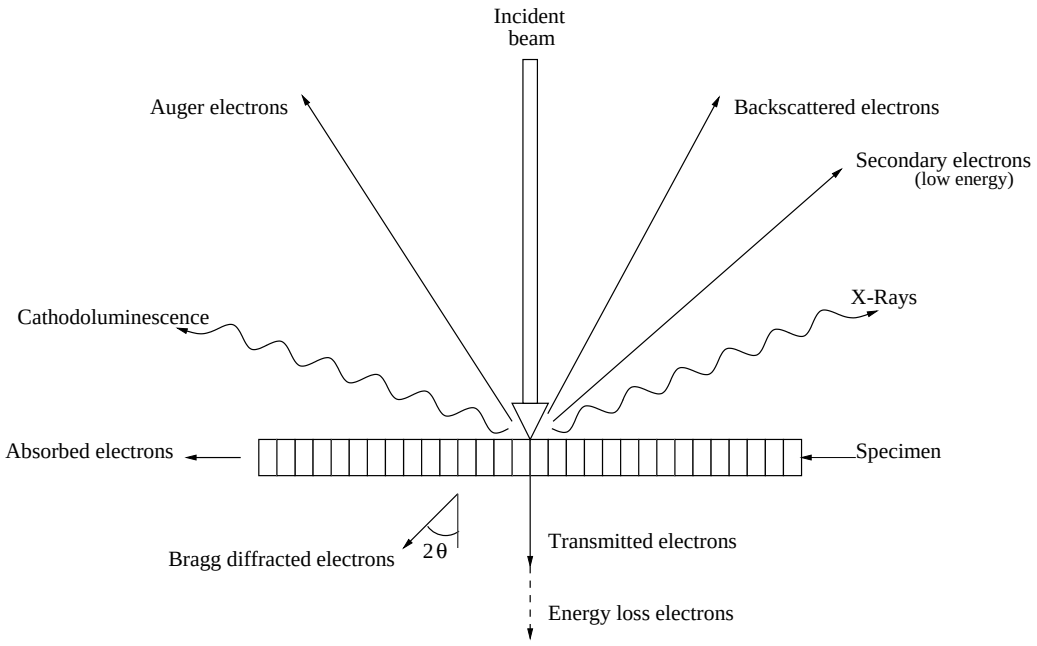

Figure 2.2: Interactions of the electron beam with the specimen. [TG79]

6. Electrons hitting the sample may cause it to emit X-rays, whose energy and wavelength is dependent on the elementary composition of the sample.

7. Electrons hitting the specimen may cause the sample to emit photons (light). This process is called cathodoluminescence.

8. Auger Electrons are the final electrons in the Auger emission process. The primary beam removes an electron from a core level of a sample atom and leaves a vacancy. Another electron falls from a higher level into the vacancy thereby releasing energy. This energy is carried of with the Auger Electron which is ejected from a higher energy level.

In a TEM the first two effects contribute to the image formation of a biological specimen.

Parts of the Transmission Electron Microscope

A substantial component of the transmission electron microscope is the electron gun. The electron gun provides a partially collimated stream of electrons of the required energy. For example, a tungsten filament is heated up to $2700°C$. Electrons are produced by thermionic emission[1] of electrons from this filament. The filament is held on a negative potential with respect to the rest of the microscope in the height of the desired energy (typically 100 - 200 keV). The electrons are accelerated through a controlling Wehnelt electrode through a hole in the anode. The Wehnelt cylinder focuses the electron stream. Further on, the electrons are focused by two condenser lenses. The area around the filament as well as the rest of the microscope is evacuated to ensure that the electrons do not lose energy in scattering processes before they hit the specimen. Improvements of the electron gun can be to use another material with a lower work function[2] for the thermionic emitter (e.g. lanthanum hexaboride). The design of the electron gun should permit adjustments of the electron beam's position and inclination. These settings are usually done by magnetic coils which also include correction for astigmatism.

The emitted electron beam now enters the condenser lens system. This modifies the beam so that the specimen is optimally illuminated. Usually two condenser lenses are used to allow a wide range of intensities for a given adjustment of the gun as well as a reduction of the illuminated area.

The specimen holder is used to move and tilt the specimen. To enable the acquisition of data sets for 3D EM, the stage has two translation modes to study different areas of the specimen at controllable positions in respect to the microscope axis and the illuminating electron beam. In addition the stage allows to tilt the specimen about at least one axis for $\pm 70°$. To maintain the vacuum the specimen is inserted through an airlock.

[1] Thermionic emission describes the process by which thermal energy is supplied to weakly bounded electrons in order to form a source of electrons.

[2] The work function describes a certain level of energy that has to be supplied to allow electrons to escape from the surface.

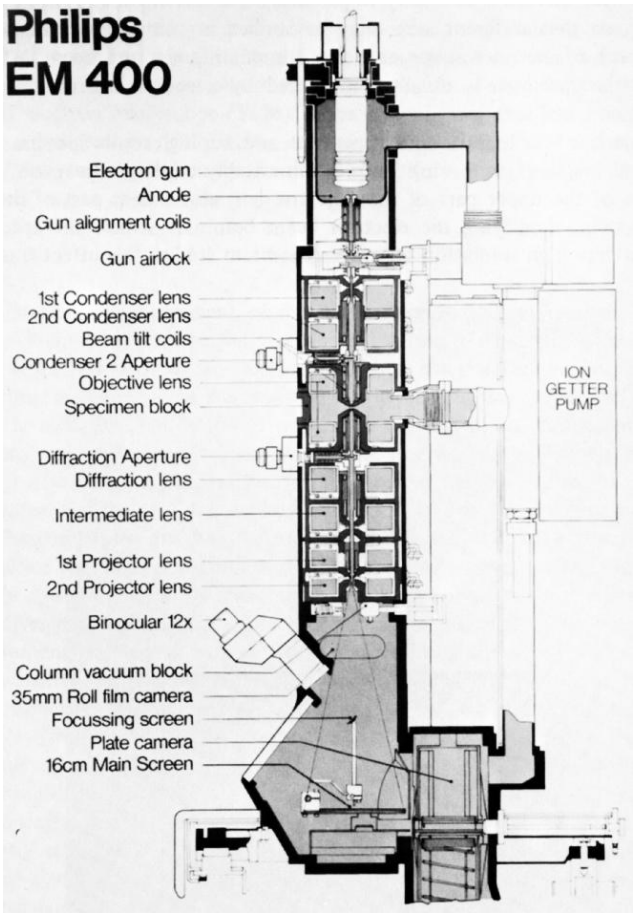

Figure 2.3: A schematic drawing of a modern TEM. [TG79]

The optical magnification system of a TEM consists of the objective lens followed by one or more projector lenses. The objective lens determines the resolution and contrast of the image. The following lenses are used to magnify the image for observation and recording. As the objective lens determines the resolving power[3] of the instrument and performs the first stage of imaging, it is the most critical lens. A high resolution objective lens has a short focal length, usually in the order of 1 - 3 mm. Normally the specimen holder is located within the objective lens so it can be part of the condenser system.

[3]The resolving power of an instrument is the resolution which can be attained under optimal viewing conditions.

There are sets of apertures in three locations:

- In the condenser system to collimate the electron beam as well as to modify its intensity;
- In the back focal plane to select electrons at a particular inclination for a later magnification;
- In the image plane to select electrons from a particular area of interest or for selected area diffraction.

The lenses are of magnetic type. They are supplied with a highly stabilized current source which is in addition variable for focusing. The lenses are designed for a high resolution, i.e. close to atomic level.

There are three major aberrations: spherical aberration (the lens fails to bring central and peripheral rays into a common focus), chromatic aberration (the lens fails to bring electrons of a different wavelength into a common focus) and astigmatism (a circle in the specimen transform to an ellipse in the image). The spherical aberration is closely related to the design and the manufacturing of the lens. Chromatic aberrations can be reduced by stabilizing the accelerating voltage and by using thin specimen, since the velocity and thus the wavelength of electrons is influenced by fluctuations in the high tension supply, and by the influence of inelastic scattering with the specimen. The wavelength of electrons is closely related to their velocity, see Eq. 2.4. Astigmatism can be corrected by the application of a compensating magnetic field.

The described parts of the TEM are shown in Fig. 2.1.

Depth of field and focus. In comparison to a light microscope the depth of field and focus is extremely large. This effect is a result of the small electron wavelength and the small angular apertures of the imaging lenses. The depth of field is the distance along the axis on the object side over which the object can be moved and still resulting in a maximally sharp image. As

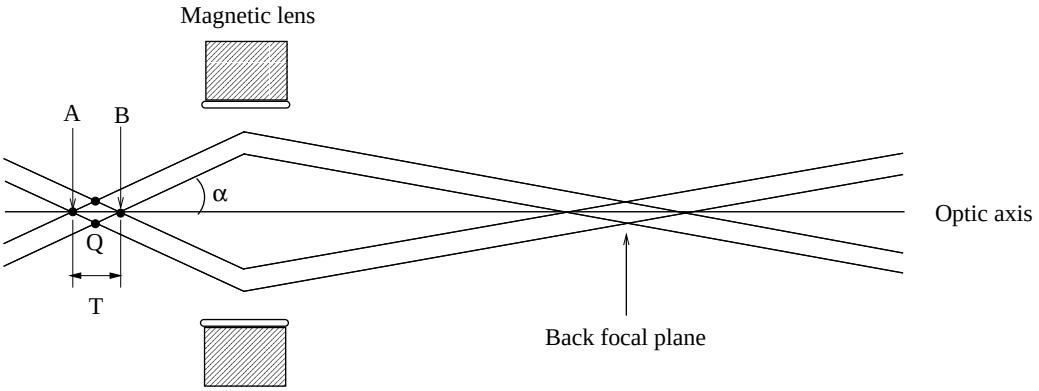

Figure 2.4: Separation of object points P and Q is the resolution limit d. Rays from these points cross the optical axis at A and B and are equally sharp. $T = A - B$ is the depth of field. [TG79]

shown in Fig. 2.4 the depth of field T is given as

$$\frac{d}{2} = \frac{T}{2} \tan \alpha, \tag{2.1}$$

where α is the lens aperture and d is the resolution, or

$$T = \frac{d}{\alpha} \qquad (\text{since } \tan \alpha \simeq \alpha \text{ for } \alpha \ll 1). \tag{2.2}$$

For $d = 1nm$ and $\alpha \simeq 2 \cdot 10^{-3} rad (\approx 1^\circ)$,

$$T = 500nm,$$

which is much larger than possible with light microscopy because in the latter α may be $1.22rad$ (70°) [TG79]. Hence for an object of $\sim \frac{1}{2}\mu m$ thickness all features of the object are focused at once, and a projection of the in focus three-dimensional object is obtained.

The depth of focus is a finite distance along the optical axis where the image appears equally sharp. The depth of focus T_f and the depth of field T are related by the magnification M, as follows [TG79]:

$$T_f = TM^2 = \frac{dM^2}{\alpha}. \tag{2.3}$$

T_f can be considered as infinite for all practical purposes, and so it is not necessary to refocus when exposing plates or film which are not located at the viewing screen.

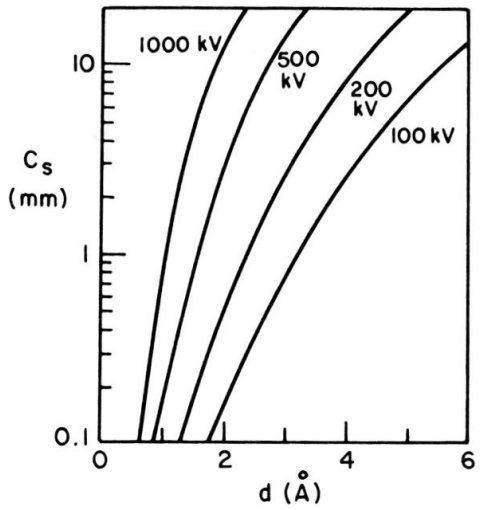

Figure 2.5: Plot showing resolution d as a function of accelerating voltage and spherical aberration coefficient C_s. [TG79]

Resolution. As mentioned before, a feature of the TEM is its high spatial resolution. The resolution is determined by the spherical aberration coefficient C_s of the objective lens and the the electron wavelength λ, given by the de Broglie wave relation:

$$\lambda = \frac{h}{mv}. \tag{2.4}$$

with h = Planck's constant, m = the electron's mass, and v = the electron's velocity.

When passing through a potential difference V an electron is accelerated to a velocity of

$$v = \sqrt{\frac{2eV}{m}}, \tag{2.5}$$

with e = charge of the electron.

Substituting Eq. 2.5 in Eq. 2.4, the wavelength of an electron is given by:

$$\lambda = \frac{h}{\sqrt{2meV}}. \tag{2.6}$$

Fig. 2.5 shows the resolution d as a function of accelerating voltage and spherical aberration coefficient C_s. If the spherical aberration coefficient is

maintained constant the resolution can be raised by increasing the accelerating voltage (through decreasing λ). So at $500kV$ or higher, atomic resolution becomes theoretically possible even in close-packed structures. The optimum voltage is determined by the specimen stability and knock-on damage and by the voltage stabilization [TG79].

2.2 Electron Tomography

Tomography is a method to reconstruct the interior of an object from its projections. Literally, the word tomography means visualization of slices. Nowadays the term electron tomography (ET) is used for any technique that utilizes the TEM to collect projections of an object and reconstructs the object and its entirety by using these projections.

To properly understand the possibility to reconstruct objects by using its projections the underlying ideas are briefly summarized.

A fundamental mathematical theorem, the so called Fourier slice theorem [Jac96], states that the measurement of a projection is equivalent to a measurement of a single central plane of the object's three-dimensional Fourier transform. The Fourier transform is an alternative representation of the object and breaks down the object's density distribution into sine waves. The following condition must be fulfilled for a complete coverage of the object in Fourier space:

- The strengths (amplitudes) and phase shifts of all sine waves traveling in all possible directions and having wavelengths down to $d/2$ have to be known, where d is the desired resolution of the three-dimensional object.

By tilting the object around a single axis through a range of $\pm 90°$, the Fourier transform is completely sampled. Here, the angular increments have to be small enough to prevent information loss. The relation between resolution d

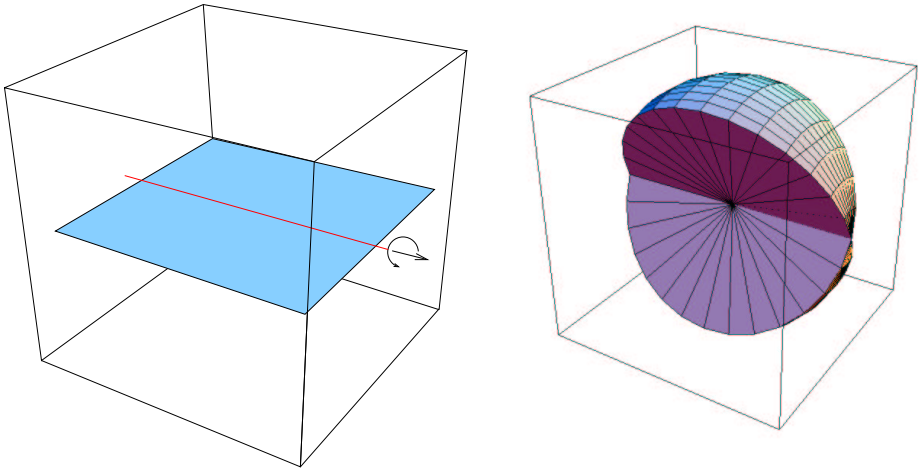

(a) Spatial domain, projections along the z-axis are taken while the plane is tilted around the axis.

(b) Missing data in the frequency domain: Since the tilt angle is mechanically restricted to $\pm 70°$, a part of the fourier transform of the object is not measured.

Figure 2.6: Single axis tilting.

and tilt angle increment $\Delta\alpha$ is given by the Crowther relation [KGT+97]:

$$d = D\Delta\alpha = \frac{\pi D}{N} \tag{2.7}$$

with D = diameter of the object, N = the number of projections recorded at equally spaced tilt angles over a range of 180°.

Due to physical limitations based on the specimen holders and the samples themselves, which are in most cases thin but large, the tilting range in electron tomography today is usually limited to $\pm 70°$. For example, a 100-nm-thick specimen at a 70° tilt angle will be 2.7 times thicker and at a 80° tilt so much as 5.7 times thicker. So a high tilt angle results in a loss of image contrast caused by multiple electron scattering. The tilt increments range from $1° - 5°$.

The limited tilting range implies that a significant part of the Fourier transform can not be measured. This is illustrated in Fig. 2.6. In Fig. 2.6(a)

a single axis tilt is illustrated. In Fig. 2.6(b) the missing spatial frequencies in Fourier space are illustrated. Due to the limited tilt angle a wedge shaped area is missing[Fra92].

Finally the series of two-dimensional data obtained is processed to obtain a three-dimensional image. For this, the 2D-images have to be aligned with respect to each other in order to refer them to a common 3-D coordinate system describing the object to be computed. Up till now, the alignment is usually done by cross-correlation [FM92] or manually. The 3D-image is then computed using a reconstruction algorithm of which several types are available, e.g. Fourier reconstruction methods, weighted backprojection methods, or iterative direct space methods. A detailed description of reconstruction methods used in ET is given in [Fra92].

2.3 Image Registration

A major delimiting factor of resolution in the 3D volume is the accuracy of alignment of the tilt series. Tomographic approaches need to acquire an image series over a large angular range (usually $\pm 70°$) with small increments (usually $1° - 5°$). The specimen can not be made perfectly eucentric. Thus specimen tilting results in both X-Y-translation and changes in focus. Although recently developed systems for automated acquisition of tilt series [KGT+97] keep track of image shifts and refocusing steps, an additional alignment step prior to the 3D-reconstruction is necessary.

Alignment. Alignment is an operation that is meant to register one or more images that contain a common motif. Due to imperfections in the tilting stage and the necessity of refocusing during the acquisition, the tilt series set has to be aligned before the 3D reconstruction. Registration and alignment are used synonymously.

Fiducial marker. As the word fiducial implies this marker is meant to be imaged reliably throughout the tilt series. In EM usually gold beads are used. Due to their high density gold beads are imaged as clearly shaped

dark spots. In the following, the markers are also referred to as gold beads or beads. During the registration, an image processing algorithm identifies features in the projections that look like beads. These features are called candidates.

Indexing. In order to align an image series it is necessary to establish a correspondence from one image to another. For this, the previously mentioned fiducial markers are used. These markers not only need to be detected in every image but also associated to a detected marker in subsequent projections. The process of associating a detected marker with its corresponding marker in the next or previous projection respectively is called indexing.

Single-axis tilting of a fiducial marker. For a perfect single-axis tilt the marker would move on an orbit with radius r around the tilt axis. As previously described TEM-images are projections along the optical axis. The orbit projected in a 2D-image results in a line that is perpendicular to the tilt axis. Line recognition is a well-known procedure in digital image processing and can be used to recognize regions of interest. The x- and y-coordinates of the marker as a function of the tilt angle result in a sinusoid according to the geometric properties of an orbit's projection.

2.4 Methods for Automatic Alignment of Tilt Series Using Fiducial Markers

At least two methods of automatic alignment of tilt series using fiducial markers have been published so far.

Fungh et al. [FLR+96] initially segment out all features throughout the tilt series that possibly represent beads. Out of the identified gold beads a set of gold beads in a reference view is interactively determined. These markers are tracked over the rest of the tilt series. This is done by a simple prediction of the position of a marker in the next projection. If a candidate is found near the predicted position, it is taken. If not enough bead positions

were found throughout the entire data stack a more vigorous search is started which again involves a prediction of the bead position. The method requires for the prediction a knowledge of the tilt axis which is not known in all cases.

Ress et al. [RHS+99] primarily specify the number of markers to be detected. Here, the threshold for each image is adjusted in a way that the predefined amount of markers were detected. The binary images containing the markers are then cross-correlated in order to obtain the relative image offsets. These offsets are used to compare the markers acquired in the reference image with those in the unindexed image. If the minimum distance of an unindexed position falls below a tolerance, the marker is accepted. The newly accepted markers now serve as the new reference. Compared to Fungh et al. the selection of candidates to track is more restrictive: Only markers detected in the zero-tilt reference were tracked.

The approach proposed in this thesis is more flexible concerning the selection of markers to be tracked. The selection is fully automatic. Furthermore, the marker must not be represented in a reference view, so it is not necessary to track a marker over the whole tilt series and it should be feasible to track markers independently tracked in the begin and end of the series. Besides, the proposed method does not require a knowledge of the tilt axis like the procedure of Fung et al. although a prediction is as well included. Thus, this algorithm should provide more flexibility and a better performance as the two previously published algorithms.

Chapter 3

Materials and Methods

3.1 Phantom Data

To verify if the rough alignment with the cross-correlation function (CCF) is working properly, a phantom data set was created using the script language RADONIS. One data set created represented a perfect single axis tilting without any shifts. In a second data set the images were shifted with respect to each other. These shifts were protocolled in a floating point.

3.2 Real Data

The data of a pore in a hyphal cell of rhizoctonia solani[1] was obtained by Bram Koster, University of Utrecht. The Philips CM120 TEM was used. The images were digitalized with a 1024^2 charge-coupled device (CCD) camera. The pixel size is $0.86nm$. As manual data collection is very time consuming an automated data collection routine was used as described in [KGT+97]. The obtained data set included 146 projections. The tilt range goes from $-66°$ up to $79°$ with an increment of $1°$. Though the data set includes images with a higher tilt angle than $70°$ and these images were taken into considaration for the later described calculations, but they do not contain

[1] Rhizoctonia solani is a plant pathogen fungus.

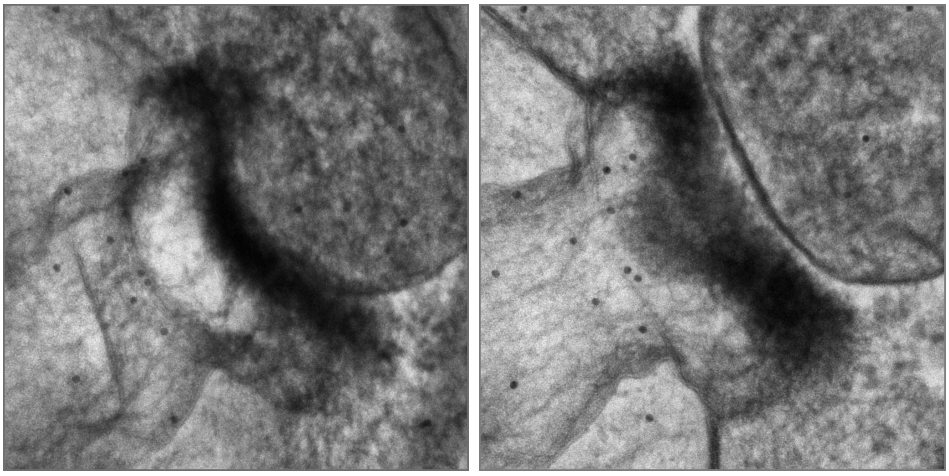

(a) −46° tilt angle **(b)** 0° tiltangle

Figure 3.1: Two projections of a pore in a hyphal cell of rhizoctonia solani.

much information due to inelastic scattering at high tilts, see p. 12.
Fig. 3.1 shows two exemplary images at different tilt angles.

3.3 Misalignment Estimation by Cross-Correlation

The cross-correlation function (CCF) can be used as a tool to roughly align projections. Here the CCF is used to eliminate major deviations.

The mathematical fundamentals are described in appendix A.

With the CCF similarities between two data sets can be found. Two successive images of the tilt series can be seen as similar but not identical sets of data. The difference that is caused by the geometric properties of tilting the object is equalized by cosine stretching prior to the computation of the CCF, see section 3.3.1. To reduce the computational burden of the CCF the images are Fourier transformed.

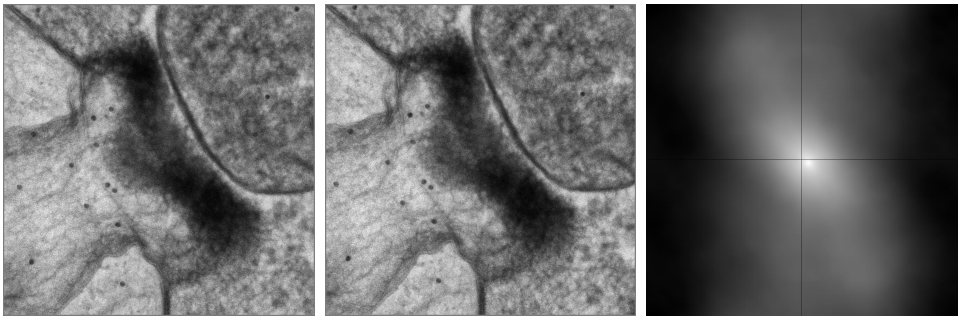

(a) $-1°$ tilt angle **(b)** $-0°$ tilt angle **(c)** CCF

Figure 3.2: Two subsequent images and their CCF.

For properly aligned images, the CCF should result in a maximum that is located in the center of the image. If the compared images are not aligned, this peak is off center. Thus the maximum's deviation from the center can be regarded as the shift vector. A shift back of the second image with respect to its correlation partner should align the two projections. This process is applied to the whole tilt series.

The correlation theorem intends the data to be periodic, which it is not in the presented case. So end effects should be considered. Since the CCF is in this case only a tool for a rough alignment, it was renounced to take care of these side effects.

In Fig. 3.2 two subsequent images with their CCF are shown. If the two images had a common origin the peak of the CCF would be located in the center of the image marked with a black cross. The displacement of this peak from the center represents the shift between the two images.

In summary, the rough alignment is implemented as follows:

The CCF of two subsequent images is calculated. Before computing the CCF a stretching factor is applied to the image with the larger absolute tilt angle. The cross-correlation is done with the aid of the fast Fourier transform (FFT). The CCF is obtained using the inverse FFT and is put into memory for a later evaluation of the image shift. The image shifts are calculated

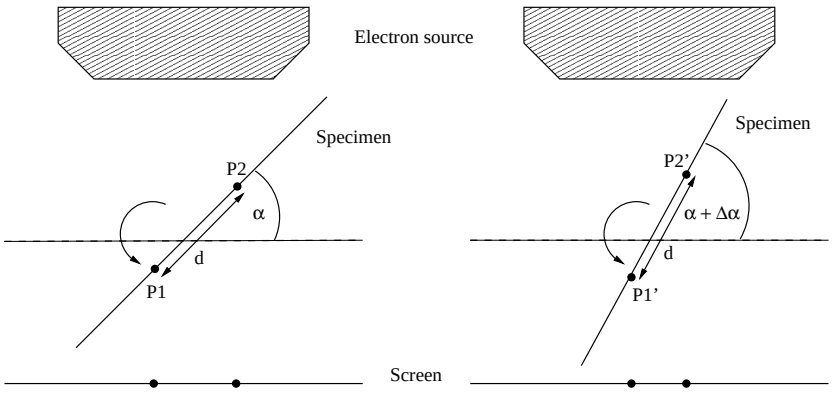

Figure 3.3: Cosine stretching: An increasing tilt angle results in a decreasing distance between the projections onto the screen of $P1$ and $P2$.

by finding the maximum of the CCF and calculating the deviation of the center. Since these vectors reveal the shift between two subsequent images, the particular image shifts are summed before shifting an image back.

3.3.1 Equalization of the Geometric Properties of Projections by Cosine Stretching

The two images correlated using the CCF are projections of the same object where the projection angle differs by $\Delta\alpha$ ($\approx 1^\circ - 2^\circ$). If $\Delta\alpha \ll 90^\circ$ the two images contain a similar but not an identical motif.

In Fig. 3.3 the projections of two different tilt angles are shown. At a higher tilt the projections of P_1 and P_2 come closer together due to the geometric properties. This effect can be equalized by cosine stretching perpendicular to the tilt axis of the projection of the higher tilt prior to the computation of the CCF which was investigated by [Guc82].

3.4 Detection of Fiducial Markers

The algorithm to detect the markers is described elsewhere [NP99]. The following outlines the basic ideas of the method and describes the outputs of the algorithm.

p_i	x_i	y_i	$s_i(pixel)$	c_i
0	263	16	11	-283.5
0	345	16	11	-283.8
0	397	18	12	-224.6
0	419	18	5	-260.7
0	63	19	6	-257.6
0	101	19	6	-311.0
0	627	19	9	-192.9
.	.	.	.	.
.	.	.	.	.
.	.	.	.	.

Table 3.1: List of detected candidates.

In principle the detection algorithm searches the image data for dark, almost circular spots and estimates the size and the local contrast of each spot. The spots are searched for using a multi-scale approach. Dark spots correspond to local minima in Laplacian convolved images if the size of the filter kernel is chosen appropriately. To estimate the size and local contrast of a spot a method is used based on a model of the marker and its properties in scale-space was developed.

The outputs of the algorithm given in Tab. 3.1 is a list of candidates C_i with the coordinates (x_i, y_i), the projection number p_i, and two quality measures, the marker size s_i (in pixel) and the local contrast c_i of a marker.

Fig. 3.4 shows several examples where the detected markers are visualized with a white cross. The number of accepted candidates can be limited by applying size or contrast thresholds. In Fig. 3.4(a) and 3.4(b) images of two different tilt angles with almost all detected features are shown, as every candidate with an estimated size above 2 pixels is marked. Fig. 3.4(c) and 3.4(d) shows the same images with thresholds chosen that only features are marked that are almost for sure a fiducial marker.

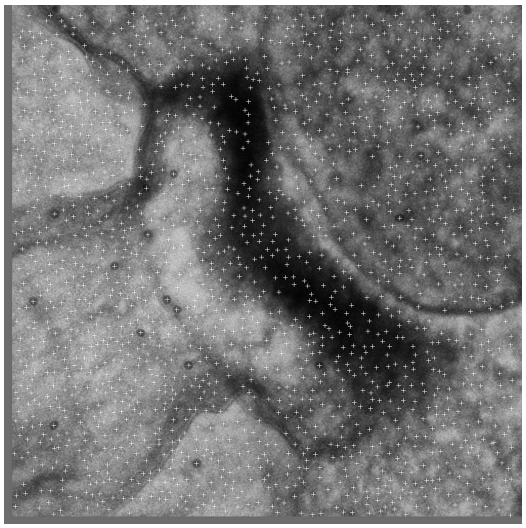

(a) $-46°$ tilt angle, markers with $s_i > 2$ and $c_i < 0$.

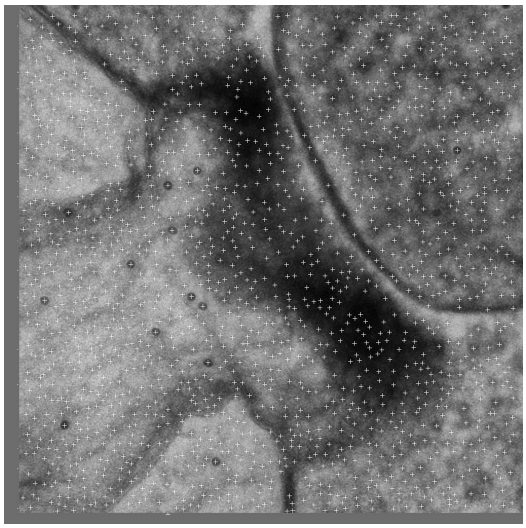

(b) $0°$ tilt angle, markers with $s_i > 2$ and $c_i < 0$.

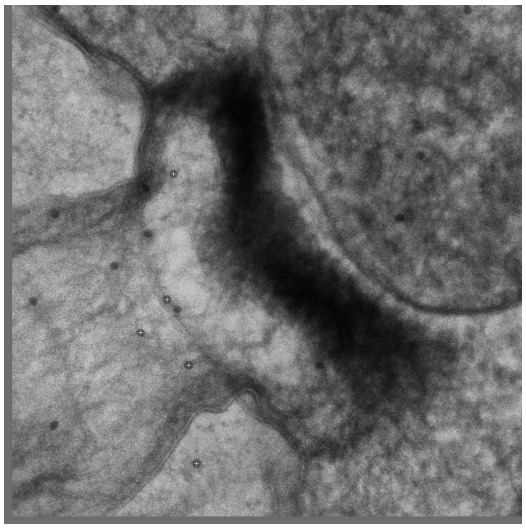

(c) $-46°$ tilt angle, markers with $s_i > 10$ and $c_i < -450$.

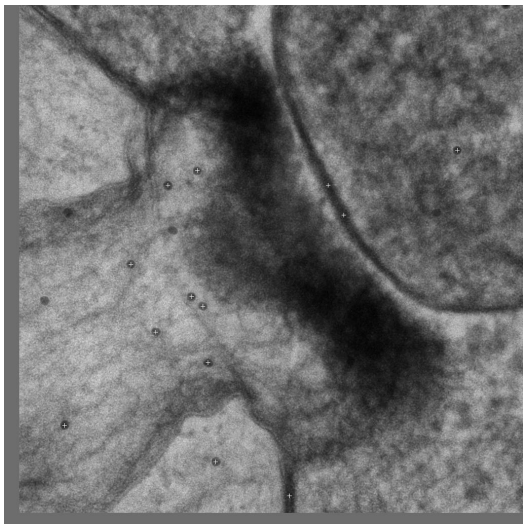

(d) $0°$ tilt angle, markers with $s_i > 10$ and $c_i < -450$.

Figure 3.4: Images with detected candidates marked with a white cross with different size or contrast thresholds applied.

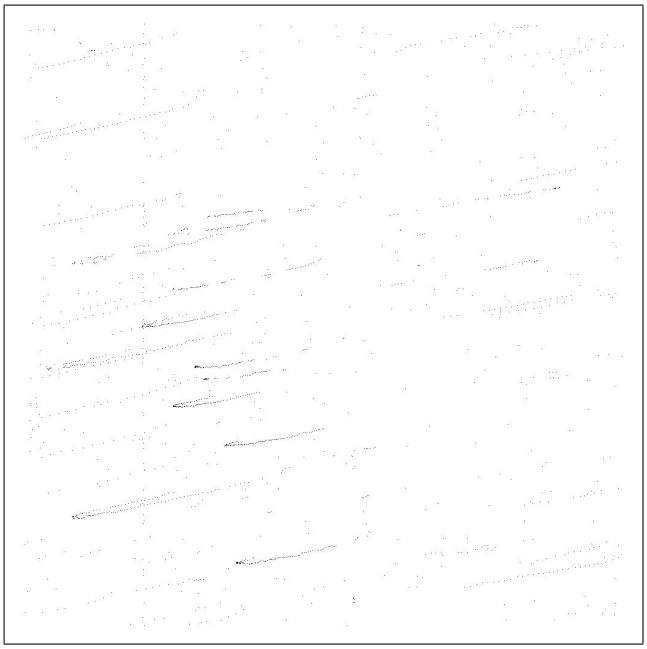

Figure 3.5: Candidates with $s_i > 10$ and $c_i < -450$ mapped onto a single image. A black dot indicates a candidate.

3.5 Marker Indexing

This section describes how the detected markers are indexed and traced over several projections. Indexing means that markers of one projection are assigned to corresponding markers in the next projection and so on. In the best case a marker can be found throughout the whole tilt series. The assignment process can be described as building up a chain of known positions throughout the tilt series.

The probability that all markers can be found throughout the whole tilt series is low, but it is possible to establish overlapping chains of markers over the tilt series.

To reduce the list of candidates a global threshold is applied. This threshold is chosen in a way that most false positive candidates are eliminated, as shown in Fig. 3.4(c) and 3.4(d). The candidates are mapped onto a single image, see Fig. 3.5.

For a perfect single axis tilt acquisition, markers move on a line perpendicular to the tilt axis. Corresponding markers of different projections approximately form a line. These lines can be recognized using the Hough-transform described later. The detected lines are utilized to determine regions of interest. Candidates located within these regions can be traced using the information obtained by the Hough transform. Thus false negative classified candidates can be found and associated to the corresponding marker.

In a first step all candidates that contribute to a found cluster are detected. The second step is to fill in any gaps existing, i.e. a marker which was detected over some projections is missing in some projections. The reason of this might be that the marker did not fulfill the applied global quality criterion or that it is located just out of the region of interest.

This can be made by either searching a defined area around the already detected marker in the next/previous projection or analyzing already indexed marker chains in a way that a prediction of the movement of one marker is possible. Then the marker is searched for in an unfiltered (i.e. there is no threshold or limitation in respect of the size) list of candidates within the defined area or at the predicted position.

3.5.1 Hough Transform

As an established tool in image processing the Hough transform [BB82] can be used to recognize lines in image space. The following approach is used. A point (x, y) in image space is passed by infinitely many lines. It is mapped onto a sinusoid defined by the points (γ, a) fulfilling the relation

$$a = \begin{pmatrix} x \\ y \end{pmatrix} \cdot \begin{pmatrix} \cos\gamma \\ \sin\gamma \end{pmatrix}, \tag{3.1}$$

which is the normal representation of a line, illustrated in Fig. 3.6 (a).

Consider a second point in image space (x, y) that also yields a sinusoidal curve in the γa-plane (parameter space). These two curves intersect in a γa-pair that corresponds to the line containing both points.

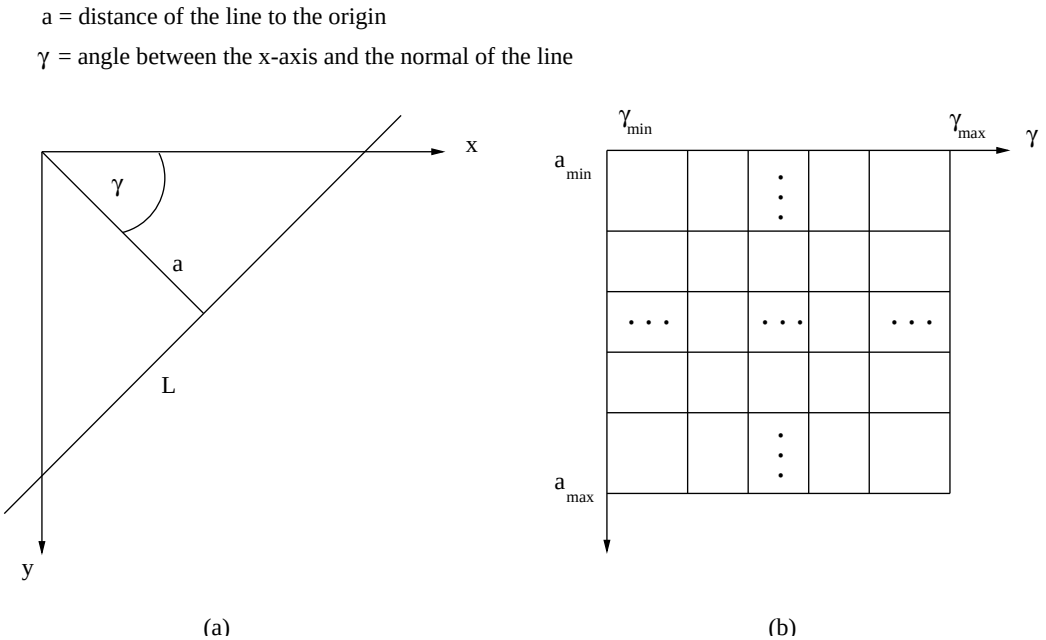

Figure 3.6: (a) Normal representation of a line L, (b) Parameter space subdivided in accumulator cells.

The parameter space is subdivided in so-called accumulator cells as illustrated in Fig. 3.6 (b).

γ is subdivided over the expected range as well as a. The cells are initially set to zero. Now γ is incremented over the selected range and equation 3.1 is solved for a. Each calculated pair is associated to its respective accumulator cell whose value is increased by one. The greater the value of an accumulator cell the more points contribute to that specific line. The accuracy of the method is defined by the number of subdivisions of the γa-plane, later on a will be parted in k accumulator cells, γ in l accumulator cells.

Fig. 3.7 presents the Hough transform of the initially chosen candidates of Fig. 3.5. As the maximum possible distance to the origin is the diagonal of the original image, a ranges from 0 to $1024\sqrt{2}$. γ ranges from 0 to $\frac{\pi}{2}$. a is subdivided in $k = 362$ and γ in $l = 180$ accumulator cells. The bright spots in the right part of the image define the detected lines in image space.

Figure 3.7: Hough transform of initially chosen candidates.

3.5.2 Determination of Regions of Interest

From the information obtained by the Hough transform clusters with promising candidates are selected. Because the images are acquired with one tilt series all the lines should have the same slope. Therefore the Hough transformation should yield a number of clearly separated maxima at the same γ. Ideally each maximum corresponds to one marker. In some cases more than one marker can contribute to the same cluster.

In order to find this γ value the absolute maximum of the Hough transform was determined, because this indicates that the most candidates are contributing to this cluster.

The Hough transform of this angle was then analyzed. Fig. 3.8 shows a typical histogram of a determined angle. The local maxima of this distribution were searched for. The first step is to apply a certain threshold. In this context this means that a minimum number of markers contributing to a line is defined. If two or more maxima are separated from each other by a

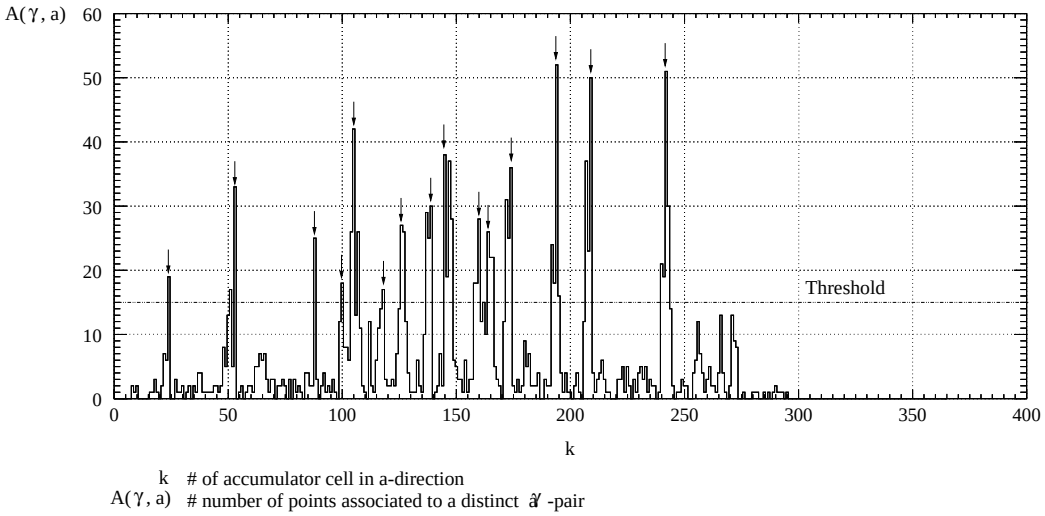

Figure 3.8: Histogram of a distinct angle in parameter space. The arrows mark the selected parameter. Threshold = 15.

minimum that itself lies above the chosen threshold, only one of these maxima is chosen to ensure the detected clusters are not too close to each other. Such a situation occurs for example for the two clusters around $a = 200$ in Fig. 3.8. Dependent on the chosen threshold clusters close to each other are not separated by a value above the threshold. So in addition it is proved if the detected lines are separated by at least two accumulator cells. This scenario appears for example for the two clusters around $a = 50$. The two clusters are separated by only one accumulator cell, so that only one is selected. In Fig. 3.8 the selected parameter is marked with an arrow. There were 15 clusters selected. Fig. 3.9 illustrates the outcome.

This method based on determining the best γ by searching for the absolute maximum does not always lead to satisfactory results. In some cases, e.g. splitting the reference images into markers with negative tilt angles or choosing a threshold that results in fewer reference points, the determined maximum leads to an angle that is not a representative of the predominant slope. This problem is shown in Fig. 3.10. The maximum determined in the Hough transform for Fig. 3.10(a) reveals a slightly steeper slope than that found for Fig. 3.10(b). In Fig. 3.10(b) the lines were clearly detected.

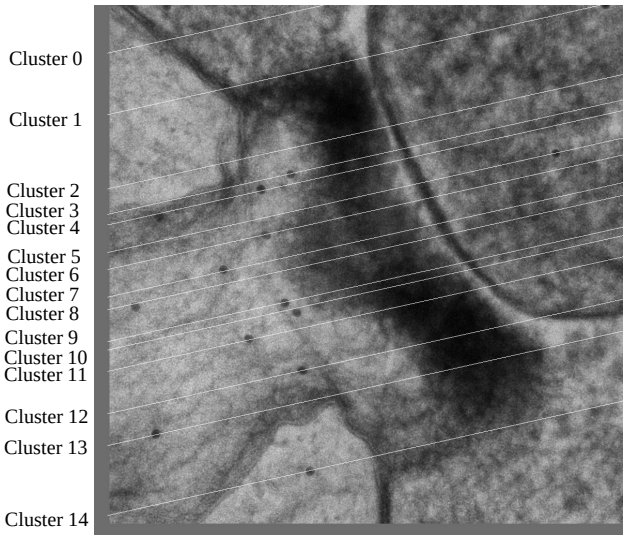

Figure 3.9: An exemplary projection of the tilt series with the selected clusters.

In Fig. 3.10(a) the detected markers do not build clear lines. The markers are lying close to each other which also results in recognizable lines in the Hough transform. In other words the slope of the line containing the most candidates is not necessarily the predominant slope.

A better method for determining the predominant slope is to find the angle γ for which the corresponding histogram obtained by the Hough transformation differs the most from an equipartition. Therefore the entropy of the histogram of every angle in the Hough transform is calculated. As mentioned in section 3.5.1, for a distinct angle γ every candidate is represented by an associated radius a, so that the number of points N_p for each angle is the same. Supposed the parameter space is subdivided in k accumulator cells per angle, the probability of a point being in the kth accumulator cell in the a-direction can therefore be calculated as

$$p_k = \frac{A_k(\gamma, a)}{N_p} \tag{3.2}$$

where $A_k(\gamma, a)$ = value of kth accumulator cell and N_p = total number of candidates that contributed to the Hough transform.

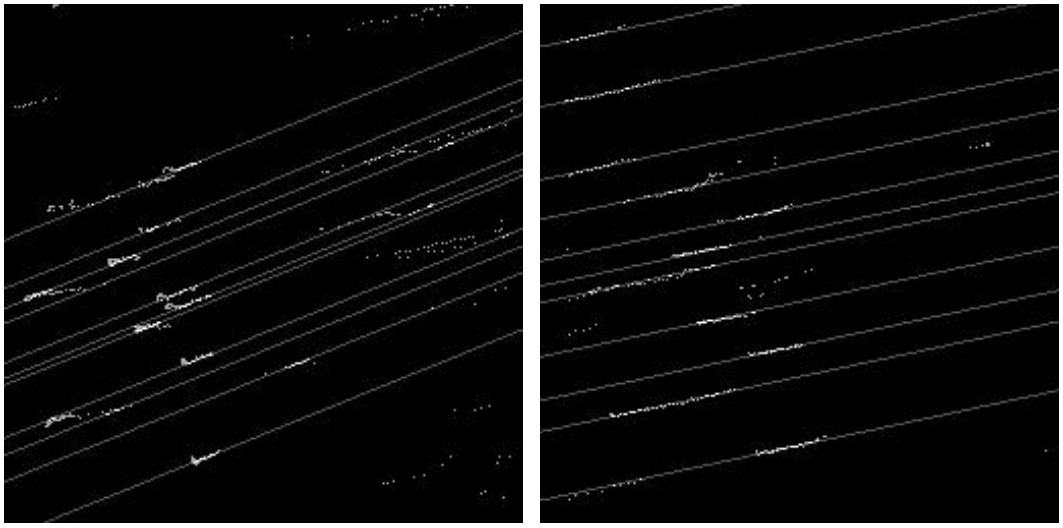

(a) Markers from $-66°$ to $0°$ tilt angle with lines indicating the selected clusters.

(b) Markers from $0°$ to $79°$ tilt angle with lines indicating the selected clusters.

Figure 3.10: Markers with selected clusters. The angle was found by determining the maximum of the Hough transform.

The entropy is calculated as

$$S = -\sum_{k=1}^{N_A} p_k ln(p_k). \tag{3.3}$$

where N_A = number of accumulator cells in a-direction.

For an equipartition applies $p_k = 1/N_A$. The entropy is therefore

$$S_e = -ln\left(\frac{1}{N_A}\right) > 0. \tag{3.4}$$

A peak results in an entropy of

$$S_p = -ln(1) = 0. \tag{3.5}$$

The more an distribution differs from an equipartition the smaller is the entropy.

The entropy of every angle in the Hough transform is calculated and the minimum entropy is searched for. This is shown in Fig. 3.11. The minimal

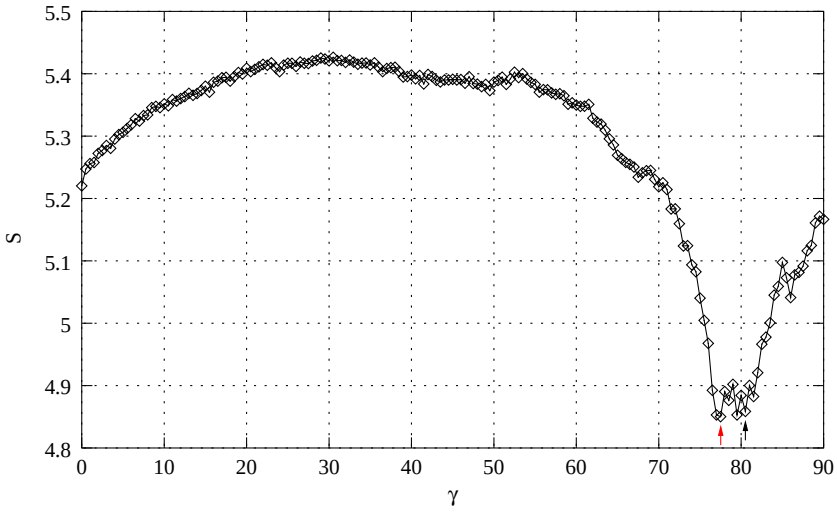

Figure 3.11: The entropy as a function of γ. The selected angle γ is labeled with a red arrow, the black arrow marks γ determined with searching for the absolute maximum.

entropy and therefore the determined angle is marked with a red arrow. The black arrow marks the angle which would have been chosen with searching for the absolute maximum in the Hough transform. After determining the predominant angle it is proceeded as described above.

The result is shown in Fig. 3.12. The cluster selection was based on the same Hough transform as in Fig. 3.10. Contrary to Fig. 3.10 the same slope was determined for both images.

3.5.3 Marker Tracing Based on the Hough Transform

Several candidates contribute to each cluster which was previously detected by the Hough transform. Typically there will be some false positive candidates contributing to the cluster and some wrongly negative classified candidates are missing. The detected clusters are now used to eliminate candidates that are not part of a cluster and to select the candidates which belong to them.

The first step is, for each projection, to search out candidates that con-

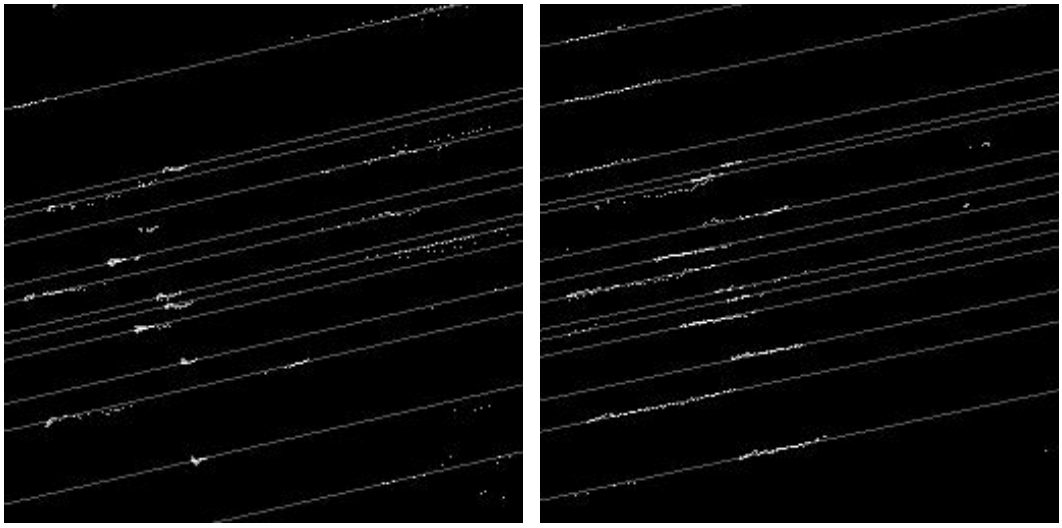

(a) Markers from $-66°$ to $0°$ tilt angle with lines indicating the selected clusters.

(b) Markers from $0°$ to $79°$ tilt angle with lines indicating the selected clusters.

Figure 3.12: Markers with selected clusters. The angle was found by determining the minimal entropy of the Hough transform.

tribute to one cluster. This is realized by creating a reference line using the parameter γ and a determined with the Hough transform. A set of reference points (x, y) is created using Eq. 3.1. This reference set is compared to the markers shown in Fig. 3.5. A candidate that is located close enough to the cluster (i.e. 5 pixels above or below the reference points), is taken. If there is more than one candidate in one projection contributing to the same cluster, the one with the higher contrast is chosen. This decision might be revised in a later step, because this candidate might not correspond to the marker that is traced at last.

The next step is to check if markers found in subsequent projections contributing to the same cluster are corresponding markers and if missing markers can be found by a search in a list of all candidates.

At first, every marker of a cluster is tested whether the marker was already detected in the next projection. If not, the unfiltered list is searched for

a candidate which is located near the already indexed marker in the next projection. The search area in x-direction is based on the indexed marker. Its x-coordinate is taken and varied over a predefined range (e.g. $\pm$ 4 pixel). The associated y-coordinate is determined with respect to the reference line. To even out the displacement of the marker in the y-direction with respect to the reference points, the distance from the marker to the reference line is calculated and considered when the search area is determined. Like the x-coordinate the y-coordinate is varied over the same range. In Fig. 3.13 the search area is illustrated for a small range of ± 2 pixel only.

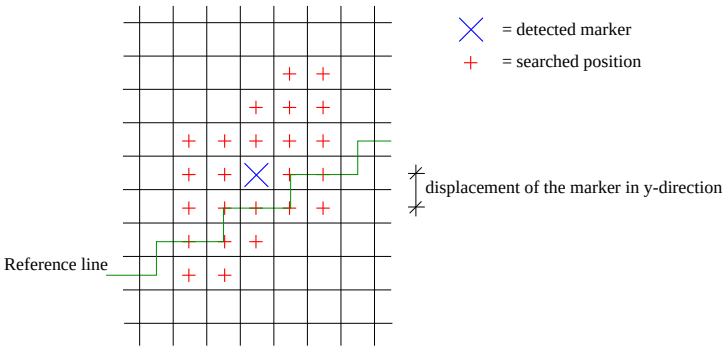

Figure 3.13: Search area. The $\times$ indicates the position of the marker already indexed in the next projection. The corresponding marker is searched for in the current projection within the area marked by red crosses.

This search is also started when the position of the indexed marker in the next projection differs by more than 20 pixels of that of the actual marker. In this case the already detected marker in the next projection contributes to this cluster but it is likely not corresponding to the marker of the previous projection.

The array is searched from 0° tilt up to the maximum positive tilt angle, then down to the maximum negative tilt angle and again up to the maximum positive tilt angle. The starting point is chosen at the 0° tilt, since the untilted projection provides the best imaging conditions so most of the markers should be able to be detected in this image.

The search is refined in the next step. This search algorithm takes ad-

vantage of the single axis projection geometry. A prediction is made where the marker is located in the next projection and this area is searched for a detected marker. The following equations are illustrated in Fig. 3.14.

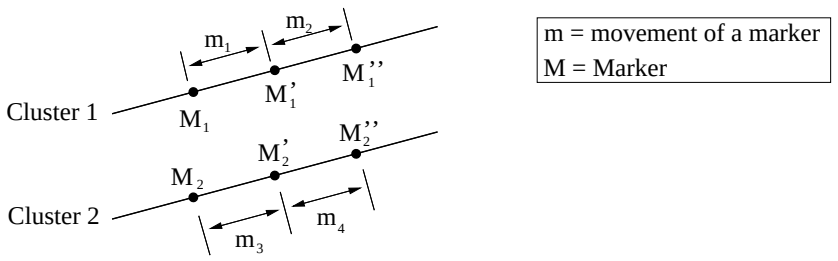

Figure 3.14: Prediction. M_1, $M_1^{'}$, $M_1^{''}$ denote the position of a marker in three subsequent projections. As the markers move on circles, there is a relation between the movement of M_1 and M_2.

The distance between two markers from one projection with the tilt angle α_3 and the same marker in the projection with the tilt angle α_4 can be calculated as

$$m_1 = r_1 \cos \alpha_3 - r_1 \cos \alpha_4. \tag{3.6}$$

where r_1 = the distance of the marker to the rotation axis, see Fig. 3.3.

Analogous to this, the movement of a second marker (which was found in projections of the same tilt angles) is calculated as

$$m_3 = r_2 \cos \alpha_3 - r_2 \cos \alpha_4. \tag{3.7}$$

Eq. 3.6 and Eq. 3.7 are solved for $\cos \alpha_3 - \cos \alpha_4$ which leads to a relation between the two rotation radii:

$$\frac{m_1}{m_3} = \frac{r_1}{r_2}. \tag{3.8}$$

The same relations are valid for m_2 and m_4.

Supposing that the marker $M_1^{''}$ has not been found yet, a prediction where this marker is located is possible with the following equation:

$$m_2 = \frac{m_1 \cdot m_4}{m_3}. \tag{3.9}$$

A prediction is only possible if two markers of subsequent projections of one cluster have already been found and if a set of already indexed markers in a second cluster is available. For ease of computation the prediction is reduced to a prediction of the movement in x-direction. The search area is ascertained as described above with the difference that the predicted x-position is taken into consideration when the x-coordinate is specified. The associated y-position is again determined with respect to the reference line. If the prediction fails because there is no cluster with three detected markers in subsequent projections or m_3 is equal to zero, the prediction routine returns the distance m_1.

Candidates that do not correspond to a traced marker but contribute to a cluster are then removed. During this step also short sets of corresponding markers are removed. Short means chains of between 3 to 6 corresponding markers.

The next step is to remove candidates which do not have a corresponding detected marker in the previous and the next projection.

In summary, tracing and indexing markers involve the following steps. First, out of the candidates that are the basis for the Hough transform (shown in Fig. 3.5), the ones close to a selected cluster are associated with this cluster. Then these markers are tracked by a simple search of a predefined area around them in the next projection. In the next step the tracking is improved by a prediction of the movement of the tracked markers. The tracking steps are followed by a removal of short chains of markers or of markers that do not correspond to the markers of the actual cluster. As the two tracking steps result in a gain of information, the tracking is repeated as long as additional markers were found.

In Fig. 3.15 the outcome of the indexing process is illustrated. The indexed markers are mapped onto a single image. The characteristic lines of a single axis tilting are recognizable.

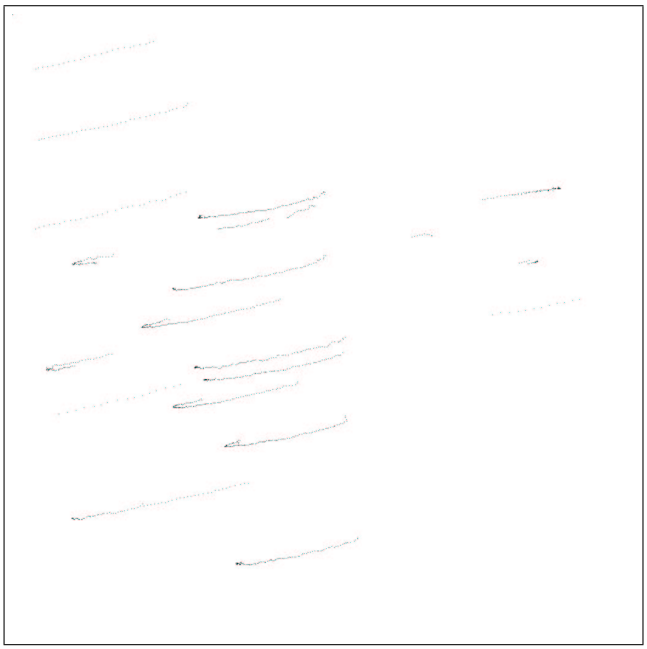

Figure 3.15: Markers which are associated to the determined clusters.

Chapter 4

Results

4.1 Simulations

The simulations served to evaluate the functionality of the CCF as a rough alignment tool.

Unshifted data. As expected the cross-correlation resulted in centered peaks. A deviation could not be detected.

Shifted data. The cross-correlation resulted in peaks deviating from the center of the image. The shift vectors were protocolled and the images were shifted back with respect to their correlation partner. A visual inspection of the aligned data set gives the impression that the data set moves like a perfect single-axis tilt, shifts are not visible. This was confirmed by examining the shift data.

4.2 Selection of Later Traced Markers

Several parameters can be changed to limit either the number of selected clusters or their distance apart. First, the accuracy of the Hough transform

can be changed by choosing the number of accumulator cells. As previously described the clusters were determined by identifying local maxima and excluding clusters that are lying next to each other in the Hough diagram. The parameter a is subdivided in $k = 362$ cells which reveals a resolution of ≈ 4 pixels. γ is subdivided in $l = 180$ cells, which is a resolution of $0.5°$. Clusters lying next to each other are excluded by the selection algorithm, with the result that clusters are separated by at least 8 pixels. The selected clusters are illustrated in Fig. 3.9.

As the selected clusters are separated by at least 8 pixels, a search area around a selected cluster of 5 pixels is justified. In Fig. 4.1 a plot of selected markers of 3 different clusters is shown. As described in Sec. 2.3, the x-position of a marker is expected to vary according to $\cos\alpha$. Thus it can be clearly seen in Fig. 4.1, that the majority of points are generated by two different markers labeled with M_1 and M_2.

In Cluster 4, two markers were already indexed throughout several projections. Some of the markers that were associated to this cluster can be clearly recognized as false positive indexed candidates. They are visualized by a surrounding circle.

A similar situation was found in cluster 8. Again mainly two markers contribute to this cluster. As mentioned on page 30, if in one projection two possible candidates were found, the one with the higher contrast is chosen. The two markers contributing to this cluster were both detected from projection # 40 till projection # 80 and both were clearly enough detected to fulfill the first global quality criteria. This plot underlines that the local contrast is not an adequate decision criteria hence both markers were selected almost equitable from projection # 42 till projection # 56.

Cluster 14 is dominated by one marker. Though a second marker was selected from projection # 110 till projection # 130 the assumption that the selected markers were chosen because of their higher local contrast is justified. This decision is revised by the tracing routines.

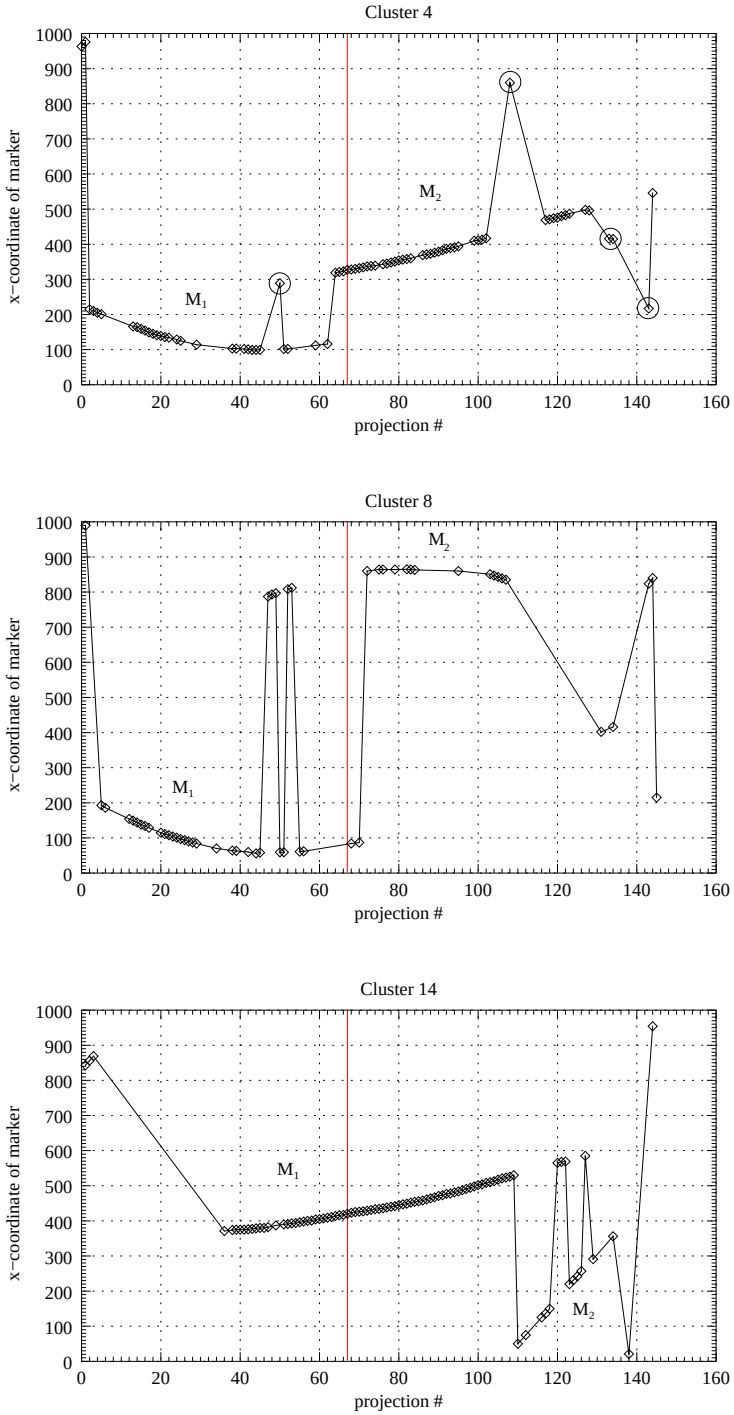

Figure 4.1: x-position of selected markers of three different clusters as a function of the projection number. The zero tilt projection is labeled with a red line.

4.3 Tracing of Markers

Tracing includes the following steps:

1. Follow the marker by searching a predefined area in either the previous or the next projection.

2. Follow the marker by predicting its position in either the previous or the next projection.

3. Remove marker chains which are too short.

The first two steps are repeated until no additional markers can be found.

The success of the first step is closely related to the radius r of the marker with respect to the tilt axis. The distance that the marker moves from one projection to another is scaled with r, see Eq. 3.6. The search area chosen is relatively small to avoid false positive markers being indexed or markers lying close to each other being wrongly associated. Some markers move in wider steps from one projection to another than what is searched by this part of the algorithm. In this case no further improvements are expected by this step. But it is to be expected that several candidates move within this range so that this step includes a gain of information that is used in the later applied prediction step. In Fig. 4.2 the improvement for the selected markers shown in Fig. 4.1 is illustrated.

For cluster 4 a significant progress of the indexing process is visible. Not only existent gaps were closed, also the indexed chain was obviously lengthened. The tracing algorithm is ended by tracing the marker from the maximal negative tilt angle up to the maximal positive tilt angle. This results in a later (i.e. higher projection #) switch from M_1 to M_2.

The situation in cluster 8 is similar. The area which was split equally between the two detected markers is now associated to one marker.

The marker of cluster 14 was after this step already indexed from projection # 15 till projection # 117. That means that the tracing resulted in around 20 candidates that were associated to this cluster and existent gaps were filled.

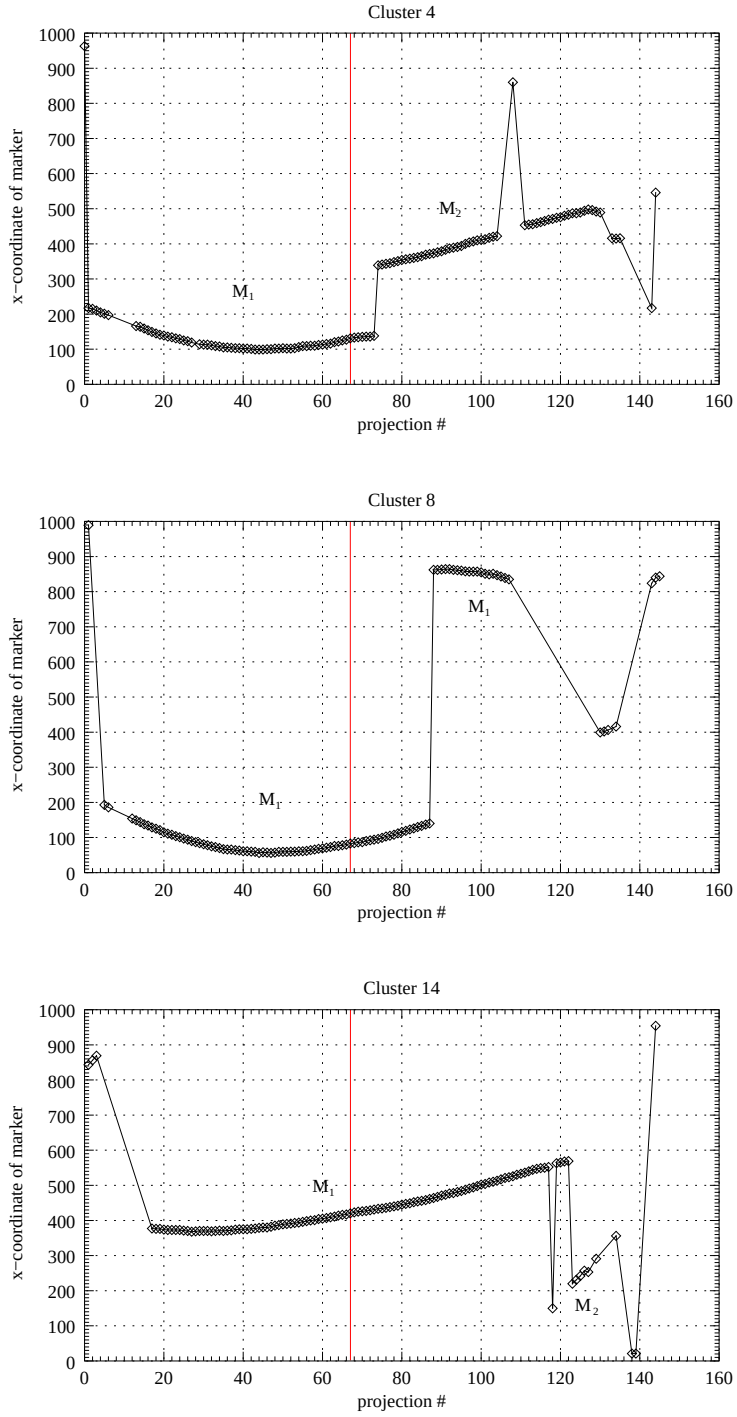

Figure 4.2: Plot of the markers after the first tracing step. The zero tilt projection is labeled with a red line.

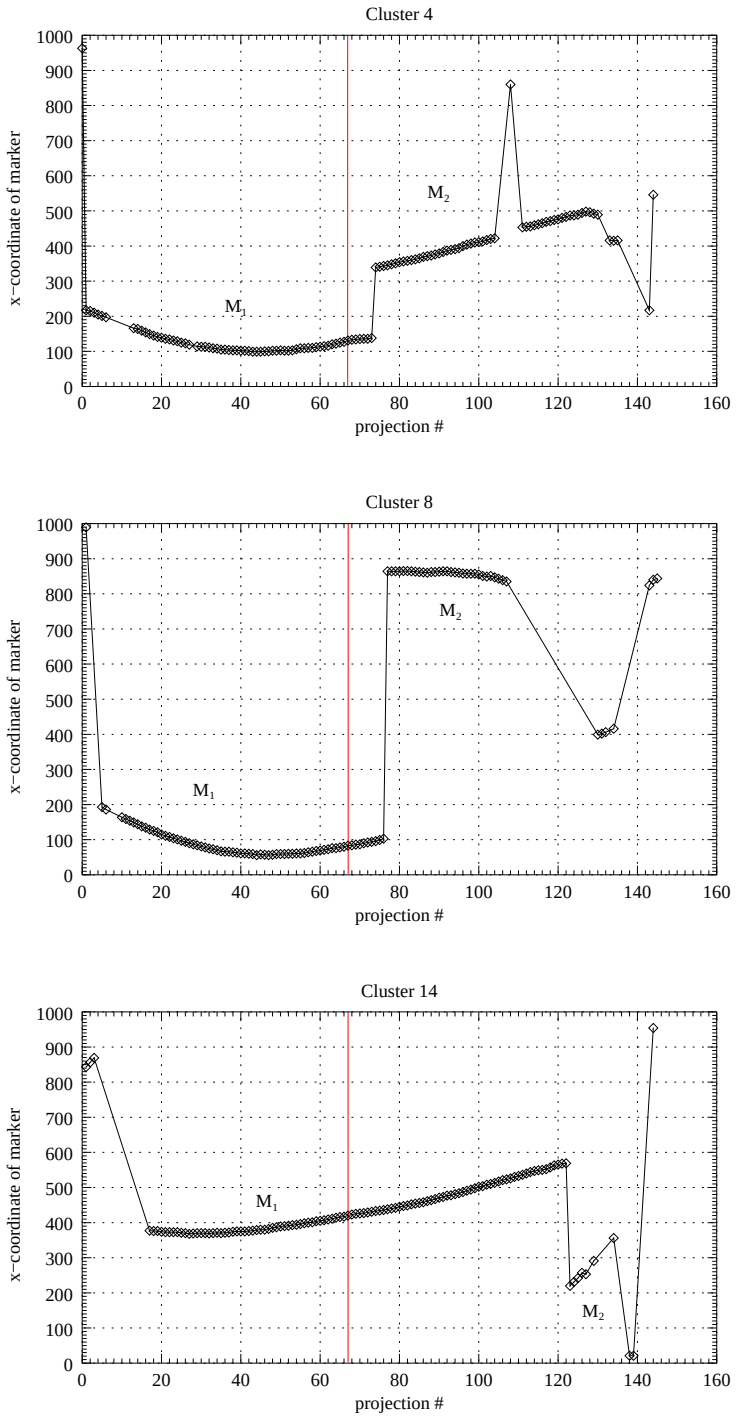

Figure 4.3: Plot of the markers after the second tracing step. The zero tilt projection is labeled with a red line.

A prediction is only possible if several conditions are fulfilled. First, the marker which the prediction is made for has to be already located and indexed for two subsequent projections followed by a gap. Second, there has to be another marker that is already indexed for the same sequence of projections.

The probability that these two conditions can be fulfilled is increased by the simple search algorithm because for some markers the search area is chosen wide enough that a gain of information was already attained. In Fig. 4.3 the result of this search is illustrated.

The search supposed by the prediction of the x-coordinate of the marker in the next/previous projection resulted in a further improvement of the indexing process. A further tracing of the markers was possible and chains throughout a large range of the tilt series were established. Existing gaps were filled.

Out of the exemplary shown clusters, both cluster 8 and 14 benefit from the prediction routine. The false positive indexed marker in cluster 14 (projection # 118) was replaced by the candidate associated to this cluster.

4.3.1 Reasons for the Failure of the Prediction

Apart from the previously mentioned problems that several conditions have to be fulfilled to make a prediction possible, the value of the prediction is still subject to restrictions. E.g. the prediction is not a proper tool for a plausibility control of indexed markers. The prediction is based on the assumption that the markers are located in a plane that also contains the tilt axis, as it is shown in Fig. 3.3. If the tilt axis is located significantly above the plane containing the markers, or if the markers do not lie in one plane, which can be the case due to the preparation, the projection of the markes do not move in phase. More precisely, a reliable prediction is only possible if the marker that serves as a reference is located in the same layer as the marker which the prediction is made for. This means markers in the same layer should move in phase.

In Fig 4.4 the movement of several markers is plotted. The markers of

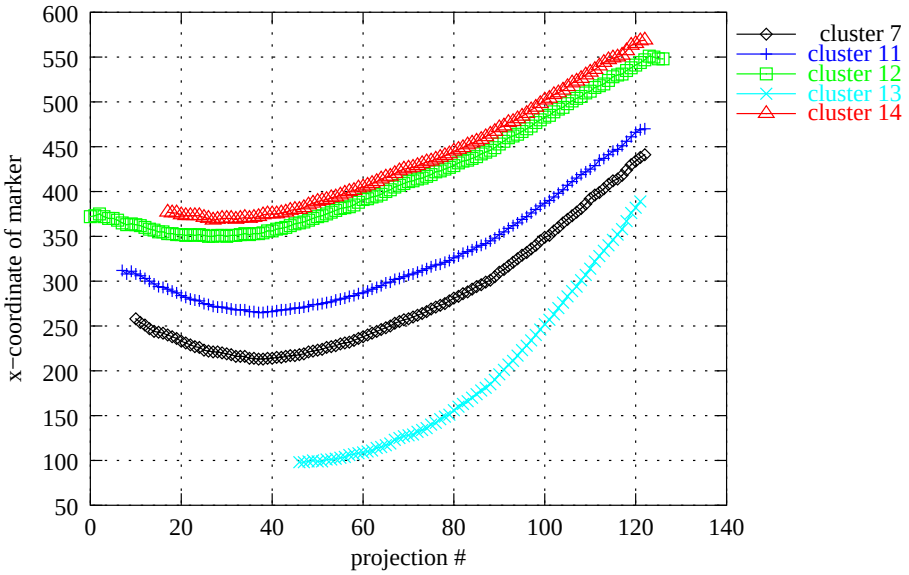

Figure 4.4: The movement of exemplary clusters throughout the tilt series in x-direction.

cluster 12 and 14 are located in the same layer since they move in phase. The same is valid for cluster 7 and 11. The marker of cluster 13 is located in another layer. The exemplary markers shown are from 3 different layers. A consequence of these phase shifts for the prediction algorithm is that only an unprecise prediction is possible, because no verification is implemented if the reference marker is located in the same layer.

4.3.2 Indexing Quality

To evaluate the indexing quality, every cluster was examined to see if the indexed chain ends due to the marker not being detected anymore or due to it not being found by the indexing algorithm. In addition, the number of repetitions necessary of the tracing steps mentioned on page 33 is determined. Finally, it was checked if markers were wrongly indexed.

A detailed description of every cluster can be found in appendix B.

Mostly the marker chains ended because of a failure of the indexing algo-

rithm. Presumably, the indexing algorithm fails because the marker in the next/previous projections was located just out of the searched area and the prediction failed either because no marker was indexed in order to serve as a reference or the prediction was based on a marker in another layer and thus misled the subsequent search.

Although most markers were indexed with one repetition, some clusters benefited from the repetition. This is illustrated for cluster 10 in Fig. 4.5. In this case the tracing was not finished until the third repetition.

In Fig. 4.6 an example for wrongly indexed candidates is given. The last indexed markers of this chain do not satisfy the expected run of the curve. These markers were also distinguished by their estimated size. This feature might serve as an elimination criteria.

4.4 Overlapping of Detected Marker Chains

Since the markers are typically not detected throughout the whole tilt series an overlap of at least one projection is necessary in order to switch the reference point for the alignment to a common origin. Therefore the ends of the chains were investigated whether there is an additional marker to switch to and whether in clusters with two or more detected markers the changeover is supported by another marker chain.

The following statements are illustrated in Fig. 4.7.

There are three clusters where more than one marker was indexed. In all three cases the changeover comes along with an overlap of at least three projections.

Cluster 0, 1, and 3 which all are only indexed for a high tilt also overlap for at least one projection with indexed chains, that they can be taken into consideration for a later alignment.

Recapitulating it is to say, that the overlap of the indexed markers is at least one projection.

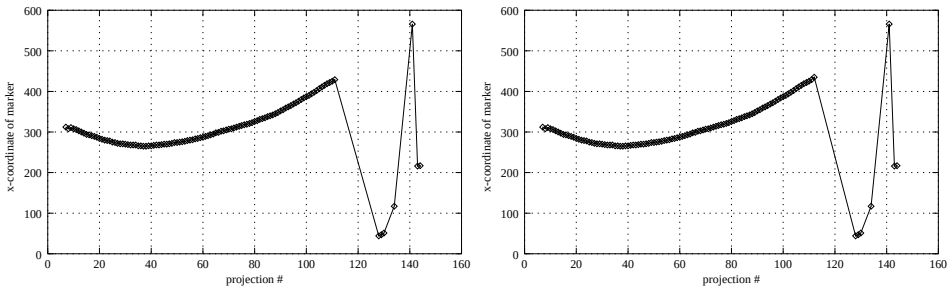

(a) Indexed Markers afterthe first flow path.

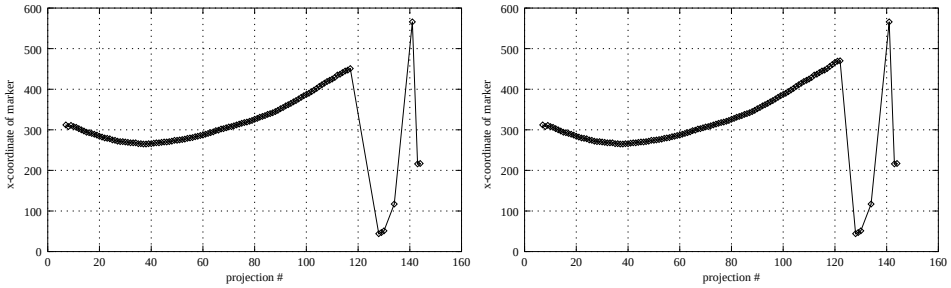

(b) Indexed markers after second flowpath.

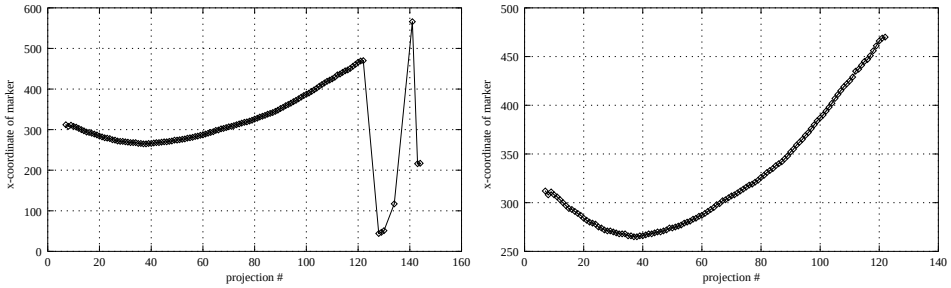

(c) Indexed markers after third flowpath.

Figure 4.5: Progress of the indexing process with recursive application of the tracing algorithms, exemplary shown for cluster 11. The left plots show the progress after the simple search algorithm, whereas the right plots show the progress after the search supposed by the prediction.

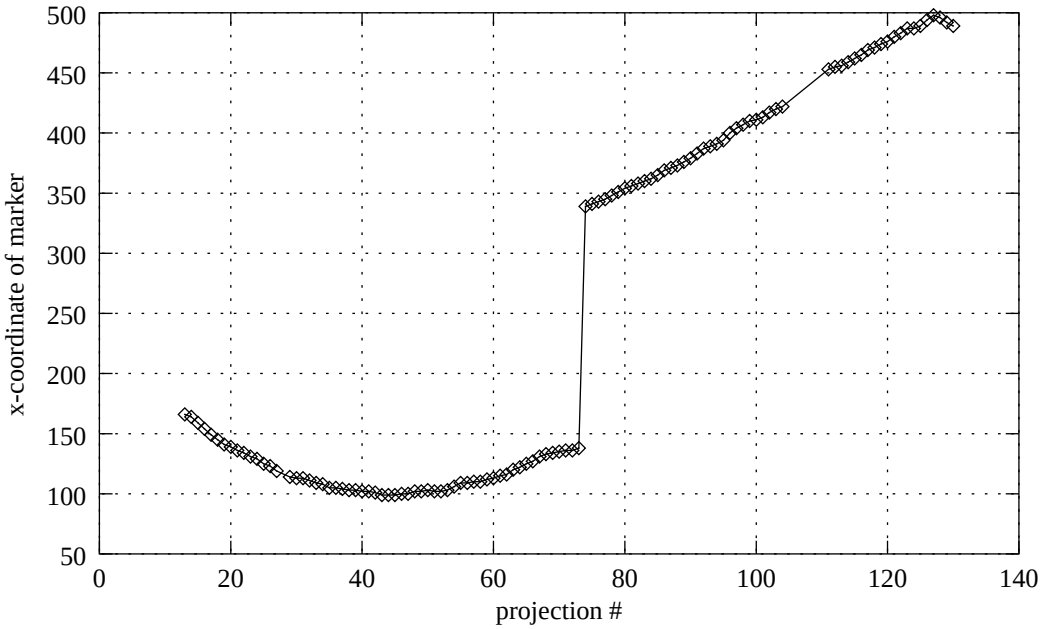

Figure 4.6: An indexed marker with some false positive indexed candidates at the end of the chain.

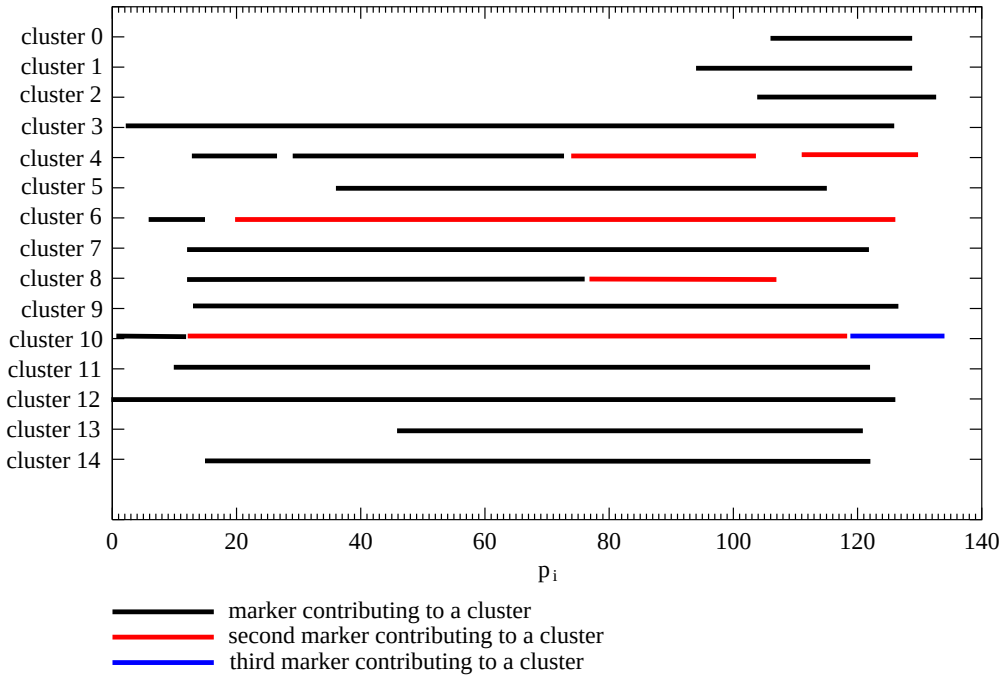

Figure 4.7: The indexed markers throughout the tilt series.

Chapter 5

Discussion

A method was developed that indexes detected fiducial markers in order to use this information for a later alignment. A goal was to develop an algorithm that needs only a minimum of interaction.
The Hough Transform is a reliable and flexible tool to select the markers to track. The selection is not restricted to markers visible in a reference view as e.g. in the approach of Ress et al. A user interaction is not necessary in contrast to Fungh et al., where the markers to track are chosen by hand. The algorithm provides to independently track markers that are only visible at the end or the beginning of a tilt series, so that markers entering and leaving the field of view are though traceable. However, the algorithm contains several parameters which are data dependent thresholds and the number of the Hough Transform's accumulator cells. The last prementioned parameter influences not only the accuracy of the Hough Transform but also the size of the search area.
Additionally, the Hough Transform provides the marker's moving direction. This is dependent on the tilt axis and the obtained information is used for the tracking algorithm. So the knowledge of the tilt axis is not a requirement for a successful tracing, as in Fung et al.
The algorithm yielded a satisfying indexing quality. Since the tracking was supposed by a prediction, the search area could be kept small. This resulted

in almost non falsely indexed marker. The analyzed outcome of the indexing algorithm showed no indexed false positive detected markers. Regardless, the indexing quality was limited, as mostly the end of a chain was caused by a failure of the indexing algorithm and not because the feature was not detected anymore. Out of the 14 selected clusters, three markers were indexed from their first to their last occurrence. In six clusters the indexing algorithm failed at a high positive tilt angle. Three cluster were unindexed at a high negative tilt angle though the feature was detected in the previous projection. For the remaining three clusters the indexing failed at both chain ends. A reason for this is that mostly the detected feature in the next projection is located outside the searched area and the prediction failed because of the prementioned reasons. In addition, at high tilts the coordinates of the detected feature were not well-centered which results in a slightly different starting point for the tracing algorithm and thus its failure.

Anyhow, the algorithm succeeded in labeling markers with the cluster they contribute to, the obtained information can be used for the alignment as e.g. published in [Law92]. Alignment algorithms need a minimum number of reference points per projection, which is provided by the presented algorithm over a large range of the tilt series.

Although the algorithm does not only track markers of a reference view, only a few markers remained indexed until high tilts. Thence some improvements are suggested in the following.

Since the correct prediction is only possible if the reference marker is located in the same layer, a verification should be implemented. This improves the indexing quality as well as this could be a tool to exclude chains of false positive detected markers.

The results showed it is possible that more than one marker is contributing to a cluster. Hence this interferes the tracking of both markers, a separate index for each marker should be established.

To improve the indexing quality of the high tilts, a second selection of clusters could be established. This means, that another reference image for the cal-

culation of the Hough Transform can be created, which is based on detected markers of high tilts. This proceeding would allow to match the applied threshold to the image features found at high tilts and therefore detect clusters only represented in high tilts.
Since the algorithm could be tested so far with only one data set, performance test with several different data sets should be carried out. A statistical evaluation of more data set could lead to a further automation of the algorithm, as it should be possible to determine thresholds automaticaly.

Chapter 6

Summary

This diploma thesis represents a method to automatically index fiducial markers. The obtained information will be used for a later alignment of the tilt series.

TEM-images acquired during a tilt series do not necessarily refer to a common origin due to the acquiring process. In order to eliminate major deviations, the data was cross-correlated. Then, the fiducial markers were detected using a feature recognition algorithm. The list of the detected features was filtered that the most false positive candidates could be eliminated. A line recognition method, the Hough transform, was used to determine regions of interest. The selected fiducial markers were tracked by either a simple search algorithm and an algorithm that utilizes the properties of single axis tilting to calculate the position of a marker in the next projection in order to associate it to an index. The indexed markers can now be used for an alignment.

The outcome of the algorithm was investigated whether the algorithm is prone to false positive indexing, and with respect to its later application. A good indexing quality was reached until hardly false positive indexed markers were investigated and the marker were indexed over a wide range of the tilt series. A limiting factor is, that only a few markers remained indexed up to tilt angles above 60°. So a starting point for further improvements is to optimize the prediction algorithm and to adopt the selection of regions of interest to the image properties in high tilts.

References

[BB82] D. H. Ballard and C. M. Brown. *Computer Vision*. Prentice-Hall, Inc., Englewood Cliff, NJ, 1982.

[FLR+96] J. C. Fung, W. Liu, W. J. De Ruijter, H. Chen, C. K. Abbey, J. W. Sedat, and D. A. Agard. Toward fully automated high-resolution electron tomography. *J. of Structural Biology*, 116:181 – 189, 1996.

[FM92] J. Frank and B. F. McEwen. *Alignment by Cross-Correlation*, pages 205 – 213. In Frank [Fra92], 1992.

[Fra92] J. Frank, editor. *Electron Tomography*. Plenum Press, New York and London, 1992.

[Guc82] R. Guckenberger. Determination of a common origin in the micrographs of tilt series in three-dimensional electron microscopy. 9:167 – 174, 1982.

[HA96] A. Hoenger and U. Aebi. 3-d reconstructions from ice-embedded and negatively stained biomacromolecular assemblies: A critical comparision. *J. of Structural Biology*, 117:99 – 116, 1996.

[Jac96] C. Jacobson. Fourier methods in 3d-reconstruction from cone-beam data, 1996.

[KGT+97] A. J. Koster, R. Grimm, D. Typke, R. Hegerl, A. Stoschek, J. Walz, and W. Baumeister. Perspectives of molecular and cel-

lular electron tomography. *J. of Structural Biology*, 120(3):276 – 308, 1997.

[Law92] M. C. Lawrence. *Least-Squares Method of Alignment Using Markers*, pages 197 – 204. In Frank [Fra92], 1992.

[MBF+95] M. Moritz, M. Braunfeld, J. Fung, J. Sedat, B. Alberts, and D. Agard. Three-dimensional structural characterization of centrosomes from early drosophila embryos. *J. of Cell Biology*, 130:1149 – 1159, 1995.

[NP99] T. Netsch and H.-O. Peitgen. Scale-space signatures for the detection of clustered microcalcifications in digital mammograms. 18(9):774 – 786, 1999.

[phi] *Einblicke in die Welt der Elektronenmikroskopie*. Philips Electron Optics.

[PTVF88] W. H. Press, S. A. Teukolsky, W.T. Vetterling, and B. P. Flannery. *Numerical Recipes in C*. Cambridge University Press, Cambridge New York Port Chester Melbourne Sydney, 1988.

[Rad88] M. Radermacher. Three-dimensional reconstruction of single particles from random and nonrandom tilt series. *Journal of Electron Microc. Tech.*, 9:359 – 394, 1988.

[RHS+99] D. Ress, M. L. Harlow, M. Schwarz, R. M. Marshall, and U. J. McMahan. Automatic acquisition of fiducial markers and alignment of images in tilt series for electron tomography. *Journal of Electron Microscopy*, 48(3):277 – 287, 1999.

[TG79] G. Thomas and M. J. Goringe. *Transmission Electron microscopy of materials*. Wiley-Intersience, New York Chichester Brisbane Toronto Singapure, 1979.

[ZPJ+94] Z. Zhou, B. Prasad, J. Jakana, F. Rixon, and W. Chiu. Protein subunit structures in the herpes simplex virus capsid from 400kv spot-scan electron cryomicroscopy. *J. Molecular Biology*, 1994.

Appendix A

Mathematical fundamentals

A.1 The Fast Fourier Transform

The Fourier transform is a powerful tool to simplify the computation of the CCF. As the word transform implies the Fourier transform is a way to represent a data set in a different way. The data can be described either in the spatial domain as a function of x, or in the frequency domain as a function of frequency f. It is possible to go back and forth between these two domains by means of the Fourier transform equations [PTVF88]:

$$\begin{aligned} H(f) &= \int_{-\infty}^{\infty} h(x) e^{2\pi i f x} dx \\ h(x) &= \int_{-\infty}^{\infty} H(f) e^{-2\pi i f x} dx. \end{aligned} \tag{A.1}$$

The fast Fourier transform is a numerical method to efficiently calculate these integrals for an equidistantly sampled function h.

A.2 The Cross-Correlation Function

The CCF of two images represented by discrete arrays i_1 and i_2 is defined as

$$\phi_{lm} = \sum_j \sum_k i_1(j,k) i_2(j+l, k+m) \tag{A.2}$$

where $i_1(j,k)$ and $i_2(j,k)$ are gray values of the respective images at point $r = (x_j, y_k)$ of a regular sampling grid [FM92].

If the two images contain a common motive in the same orientation but at different positions r_1 and r_2 the CCF shows a peak in a position described by the shift vector $\Delta r = r_1 - r_2$.

In practice, the computation of the CCF does not follow Eq. A.2. It is speeded up by the use of the convolution theorem:

$$\phi_{lm} = \mathcal{F}^{-1} \left\{ \mathcal{F} \left\{ i_1 \right\} \mathcal{F}^* \left\{ i_2 \right\} \right\}. \tag{A.3}$$

$\mathcal{F}$ and $\mathcal{F}^{-1}$ denote the discrete forward and reverse Fourier transformation, and $*$ denotes the use of the complex conjugate of the expression.

Appendix B

Marker tracing

After the automatic detection, every cluster was examined manually to see whether the chains end because of failures of the algorithm or because the feature disapears. Therefore the full list of candidates was searched, the coordinates the candidate should be located was estimated by a visual inspection of the data set.
In the following, the properties of each cluster are summarized.

Cluster 0. One marker contributes to this cluster. The indexing is concluded after the first flow path of the tracing steps. The marker is indexed from its entering of the field of view. It was detected in the subsequent projection behind the last indexed marker, but this candidate could not be associated with this cluster.

Cluster 1. One marker contributes to this cluster. The indexing is concluded after the first flow path of the tracing steps. The marker is indexed from its entering of the field of view. It was detected in the subsequent projection behind the last indexed marker, but this candidate could not be associated with this cluster.

Cluster 2. One marker contributes to this cluster. The indexing is concluded after the first flow path of the tracing steps. The marker is indexed from its entering of the field of view. It was detected in the subsequent

projection behind the last indexed marker, but this candidate could not be associated with this cluster.

Cluster 3. One marker contributes to this cluster. The indexing is concluded after the first flow path of the tracing steps. The marker is indexed from the projection of its first detection on. It was detected in the subsequent projection behind the last indexed marker, but this candidate could not be associated with this cluster.

Cluster 4. Two markers contribute to this cluster. The indexing is concluded after the first flow path of the tracing steps. The marker was already detected before the first indexed position. A shorter chain of this marker was indexed but removed as the association to the finally indexed chain was not possible. From projection # 74 on the second marker was indexed. The indexing was interrupted in projection # 105. Though the marker was detected it was not indexed. It was indexed again later on (i.e. at a higher tilt), though the marker was detected before it was indexed. This last chain ended up at a high tilt, where the marker could not be detected anymore.

Cluster 5. One marker contributes to this cluster. The indexing is concluded after the second flow path of the tracing steps. The marker was already detected before the first indexed position. It was detected in the subsequent projection behind the last indexed marker, but this candidate could not be associated with this cluster.

Cluster 6. Two markers contribute to this cluster. The indexing is concluded after the second flow path of the tracing steps. The marker was indexed from the first projection it was detected in. The marker was detected in the subsequent projection behind the last indexed marker, but this marker could not be associated with this cluster.

Cluster 7. One marker contributes to this cluster. The indexing is concluded after the first flow path of the tracing steps. It was already detected before the first indexed position. It was detected in the subsequent projection behind the last indexed marker, but this candidate could not be associated

with this cluster.

Cluster 8. Two markers contribute to this cluster. The indexing is concluded after the first flow path of the tracing steps. The marker was already detected before the first indexed position. From projection # 77 on the second marker was indexed. The chain ended up at a high tilt, where the marker could not be detected anymore.

Cluster 9. One marker contributes to this cluster. The indexing is concluded after the first flow path of the tracing steps. The marker was already detected before the first indexed position. The chain ended up at a high tilt, where the marker could not be detected anymore.

Cluster 10. Three markers contribute to this cluster. The indexing is concluded after the third flow path of the tracing steps. The first marker is indexed from the projection of its first detection on. From projection # 13 on the second marker was traced. This marker was indexed until it was not detected anymore. From that projection on the third marker was traced. This last chain ended up at a high tilt, where the marker could not be detected anymore.

Cluster 11. One marker contributes to this cluster. The indexing is concluded after the third flow path of the tracing steps. The marker was already detected before the first indexed position. It was detected in the subsequent projection behind the last indexed marker, but this candidate could not be associated with this cluster.

Cluster 12. One marker contributes to this cluster. The indexing is concluded after the first flow path of the tracing steps. The marker was indexed from the first projection on. The chain ended up at a high tilt, where the marker could not be detected anymore.

Cluster 13. One marker contributes to this cluster. The indexing is concluded after the first flow path of the tracing steps. The marker was indexed from the first projection it was detected in. The chain ended up at a high tilt, where the marker could not be detected anymore.

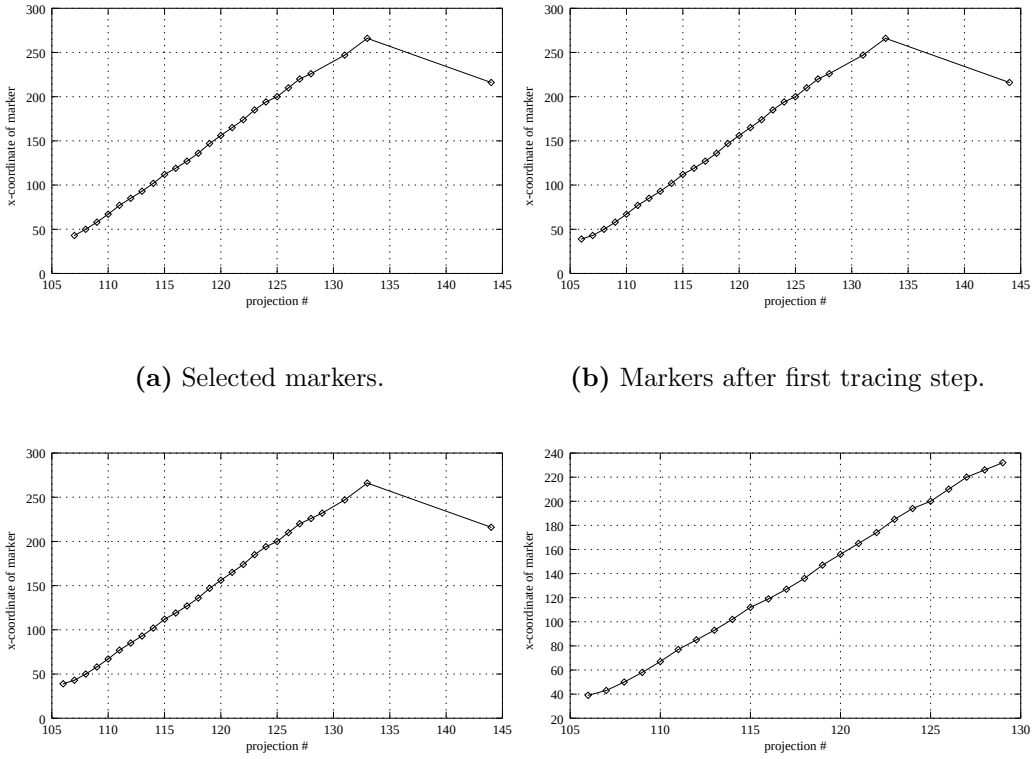

(a) Selected markers.

(b) Markers after first tracing step.

(c) Markers after second tracing step.

(d) Finally indexed markers.

Figure B.1: Cluster 0.

Cluster 14. One marker contributes to this cluster. The indexing is concluded after the first flow path of the tracing steps. The marker was indexed from the first projection it was detected in. It was detected in the subsequent projection behind the last indexed marker, but this candidate could not be associated with this cluster.

In the following the distinct steps of the indexing process are visualized for each cluster.

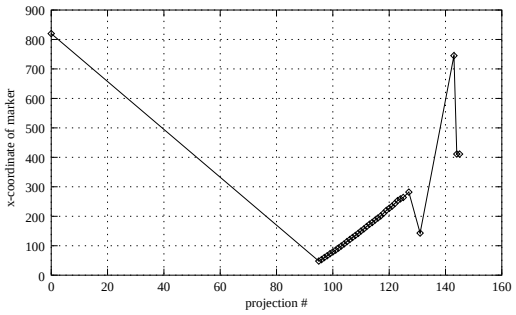

(a) Selected markers.

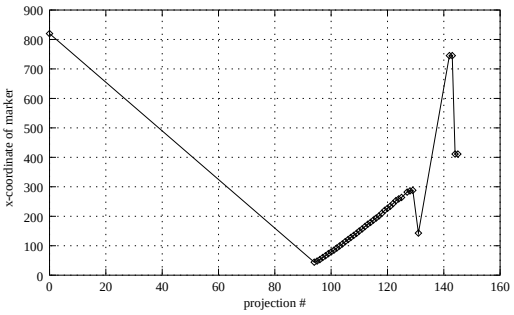

(b) Markers after first tracing step.

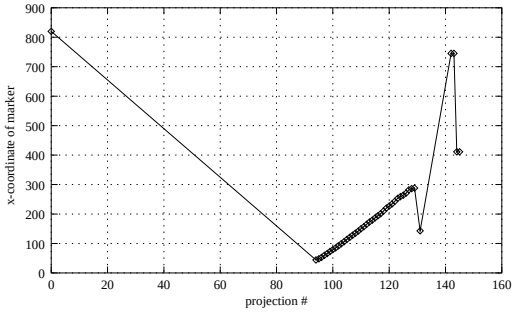

(c) Markers after second tracing step.

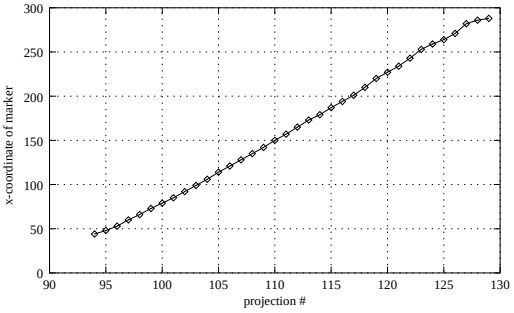

(d) Finally indexed markers.

Figure B.2: Cluster 1.

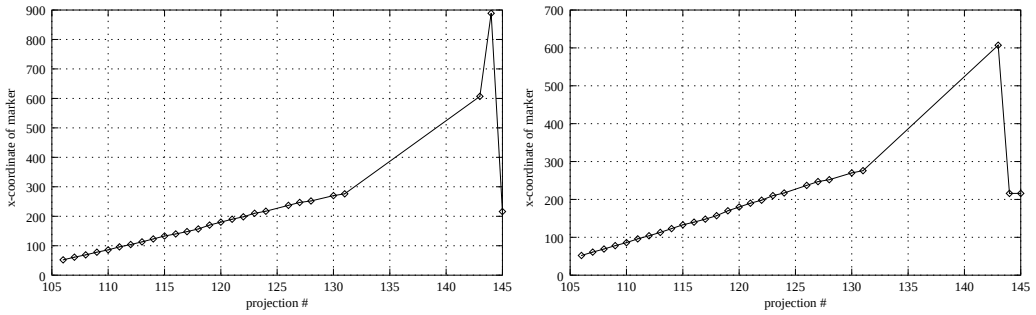

(a) Selected markers.

(b) Markers after first tracing step.

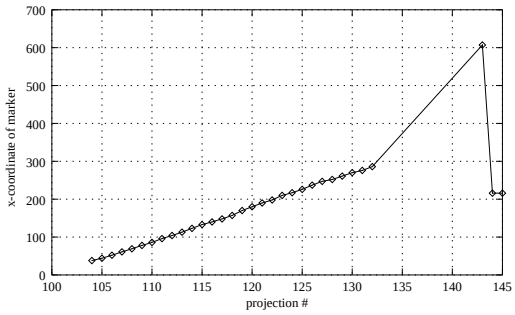

(c) Markers after second tracing step.

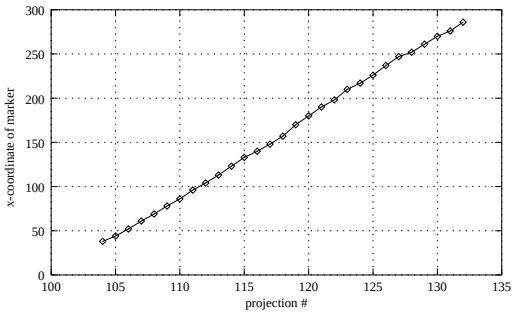

(d) Finally indexed markers.

Figure B.3: Cluster 2.

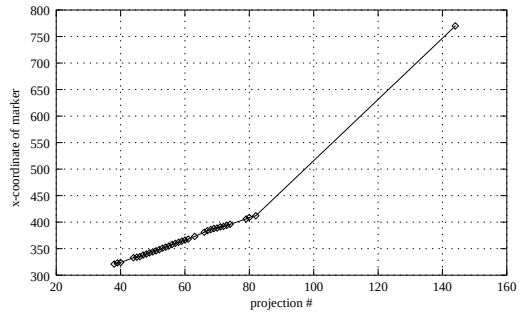

(a) Selected markers.

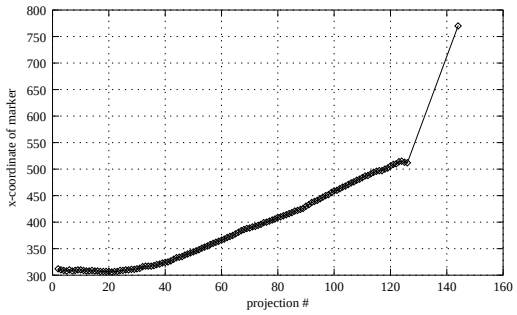

(b) Markers after first tracing step.

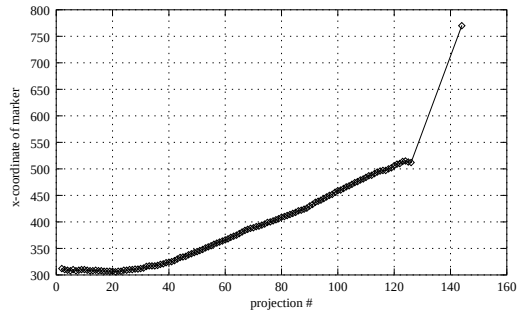

(c) Markers after second tracing step.

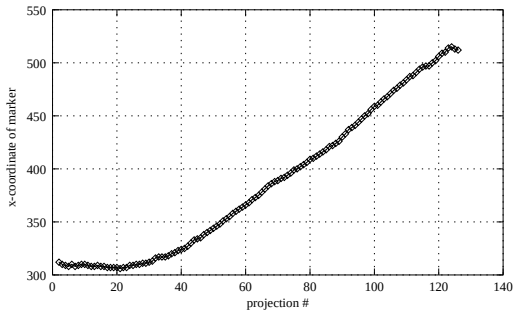

(d) Finally indexed markers.

Figure B.4: Cluster 3.

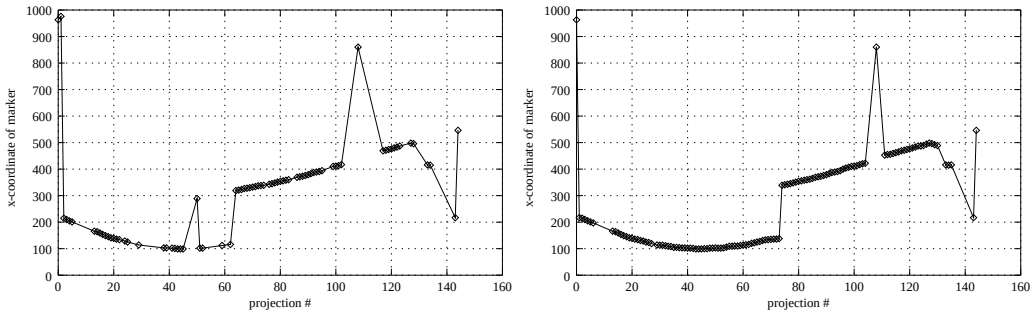

(a) Selected markers.

(b) Markers after first tracing step.

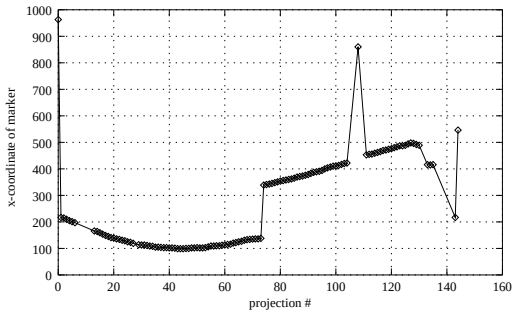

(c) Markers after second tracing step.

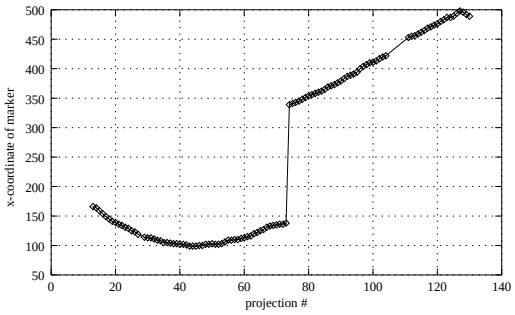

(d) Finally indexed markers.

Figure B.5: Cluster 4.

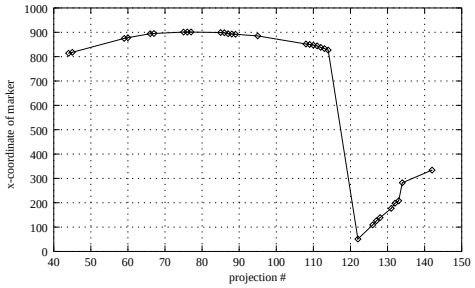

(a) Selected markers.

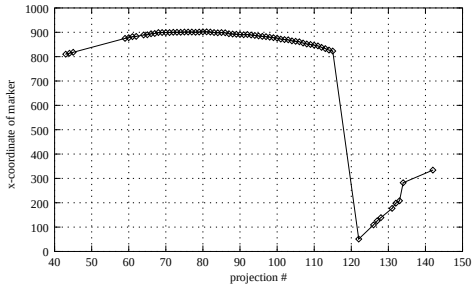

(b) Markers after first tracing step.

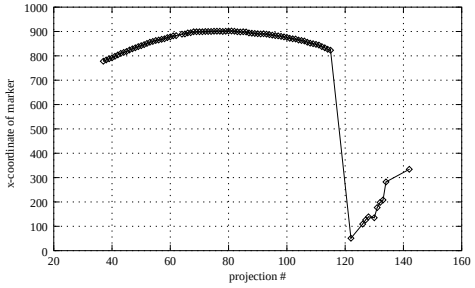

(c) Markers after second tracing step.

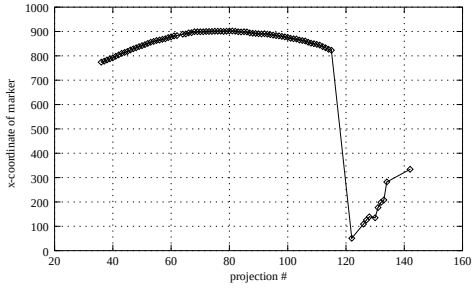

(d) Markers after third tracing step.

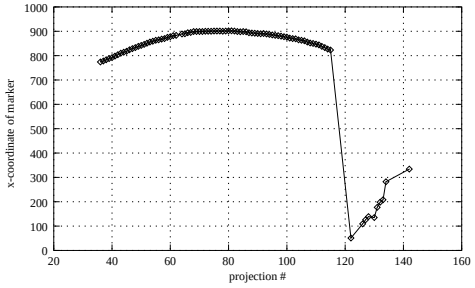

(e) Markers after forth tracing step.

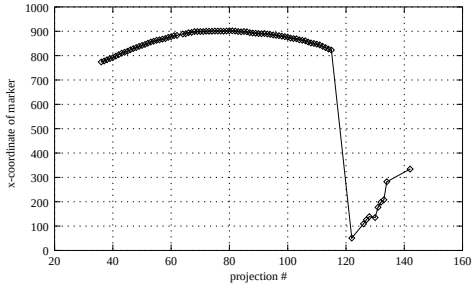

(f) Markers after fifth tracing step.

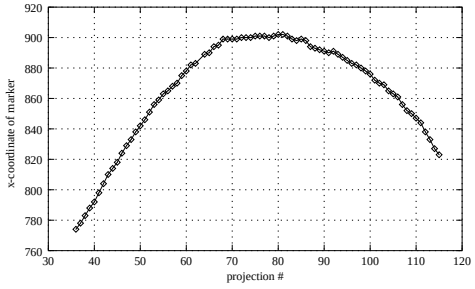

(g) Finally indexed markers.

Figure B.6: Cluster 5.

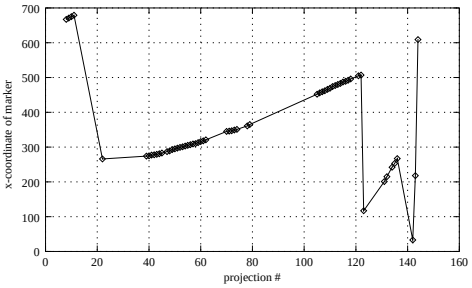

(a) Selected markers.

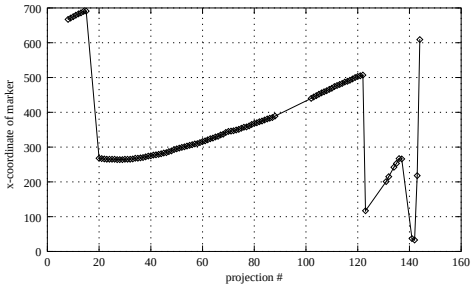

(b) Markers after first tracing step.

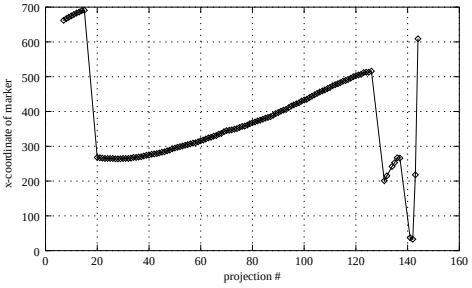

(c) Markers after second tracing step.

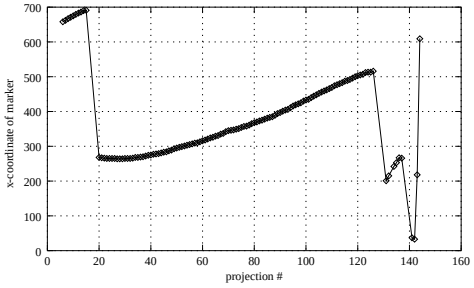

(d) Markers after third tracing step.

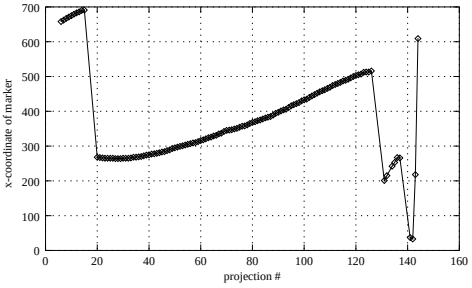

(e) Markers after forth tracing step.

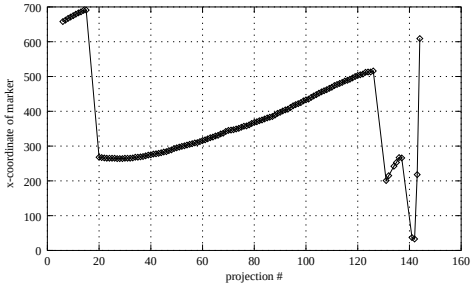

(f) Markers after fifth tracing step.

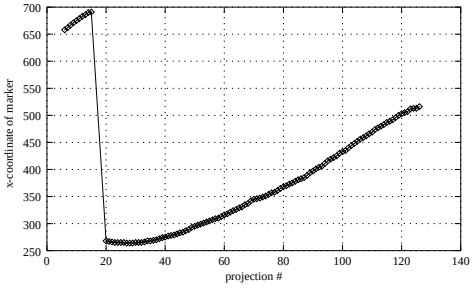

(g) Finally indexed markers.

Figure B.7: Cluster 6.

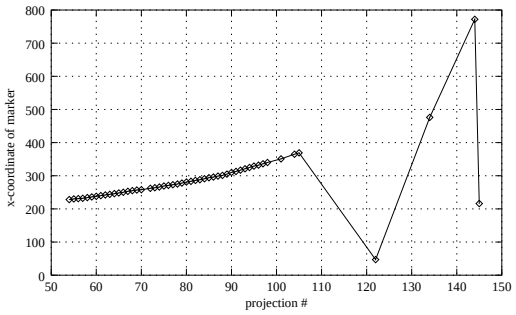

(a) Selected markers.

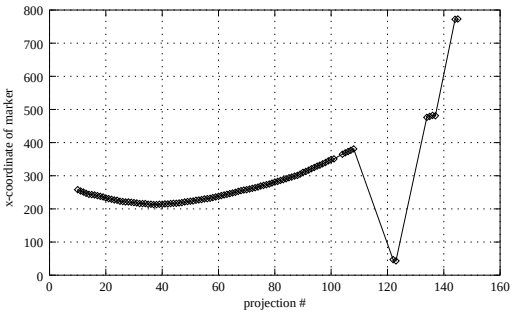

(b) Markers after first tracing step.

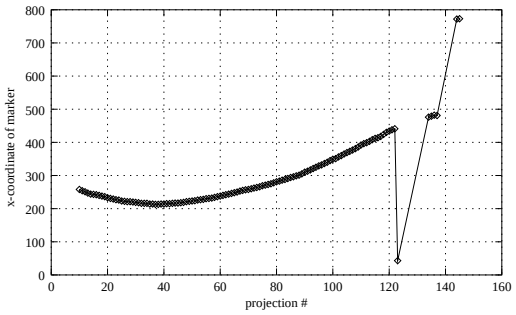

(c) Markers after second tracing step.

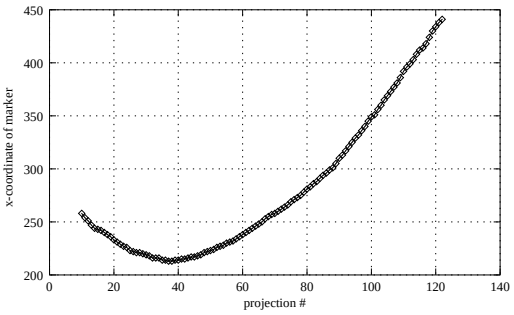

(d) Finally indexed markers.

Figure B.8: Cluster 7.

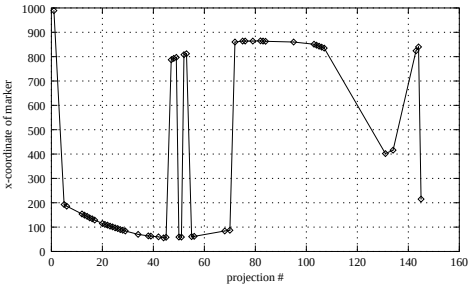

(a) Selected markers.

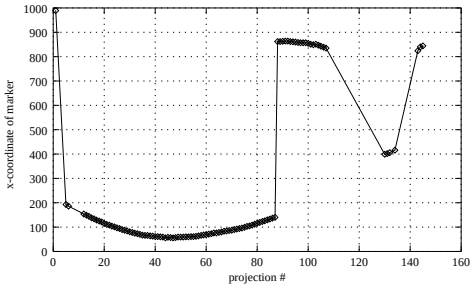

(b) Markers after first tracing step.

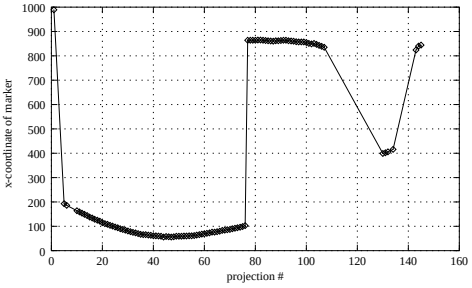

(c) Markers after second tracing step.

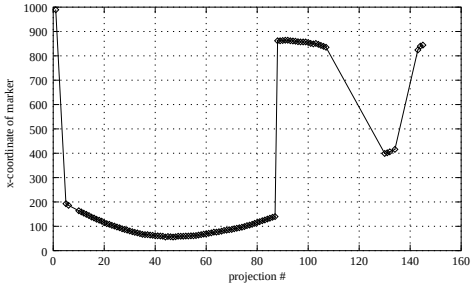

(d) Markers after third tracing step.

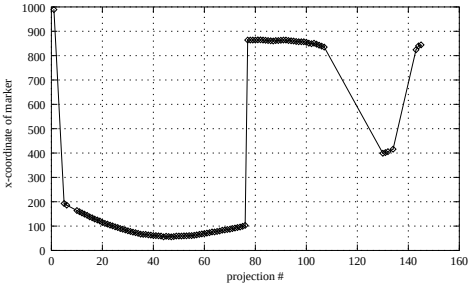

(e) Markers after forth tracing step.

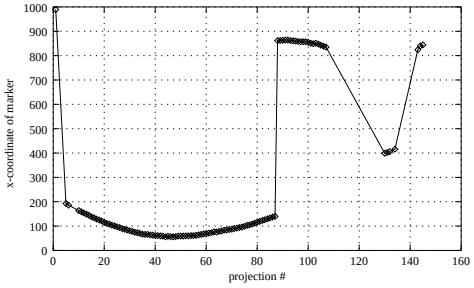

(f) Markers after fifth tracing step.

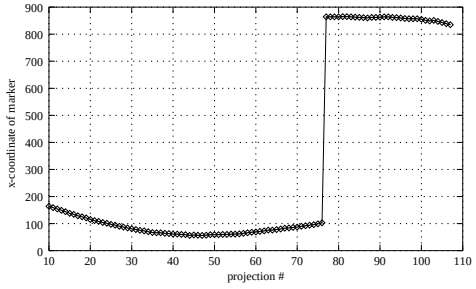

(g) Finally indexed markers.

Figure B.9: Cluster 8.

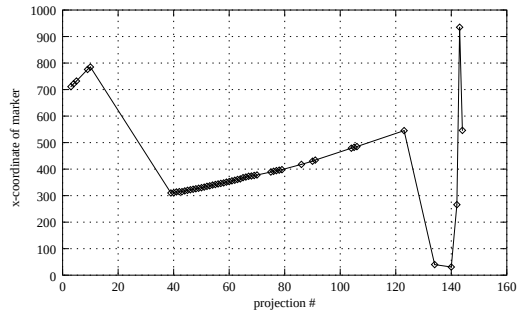

(a) Selected markers.

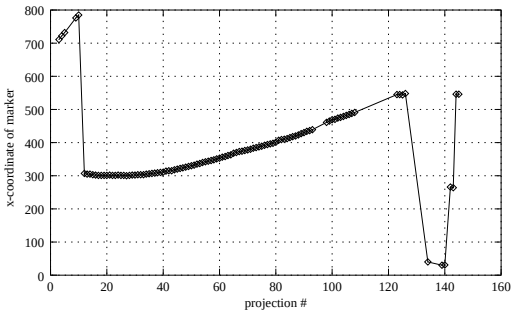

(b) Markers after first tracing step.

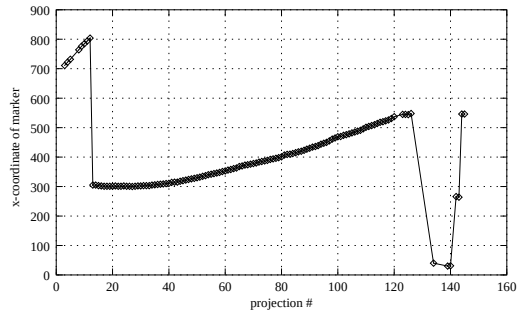

(c) Markers after second tracing step.

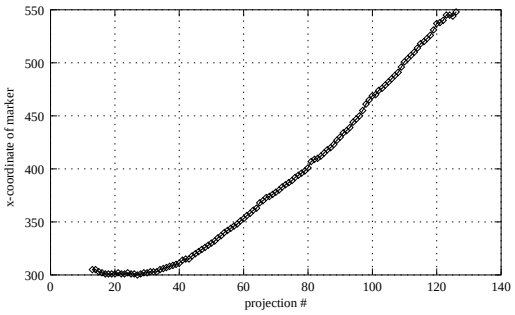

(d) Finally indexed markers.

Figure B.10: Cluster 9.

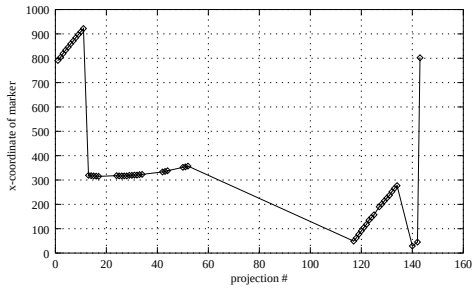

(a) Selected markers.

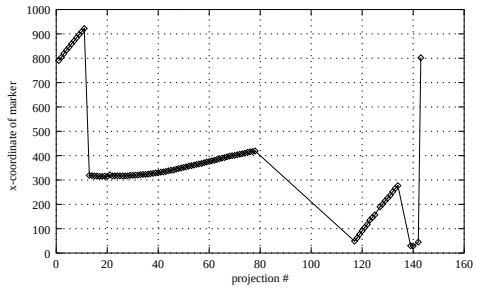

(b) Markers after first tracing step.

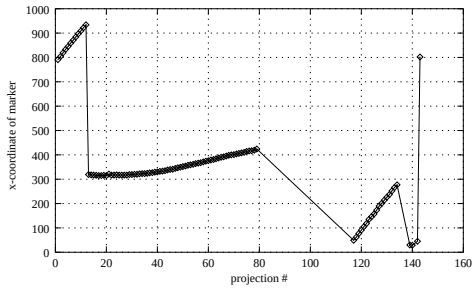

(c) Markers after second tracing step.

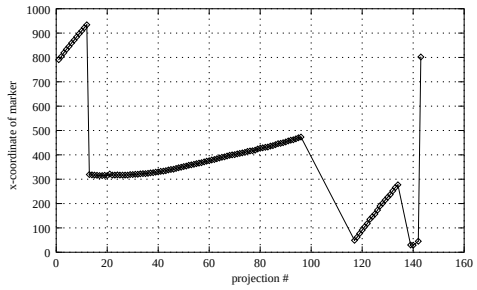

(d) Markers after third tracing step.

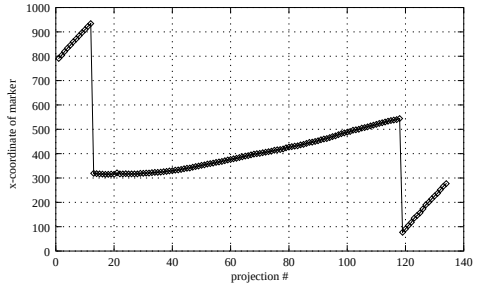

(e) Finally indexed markers.

Figure B.11: Cluster 10.

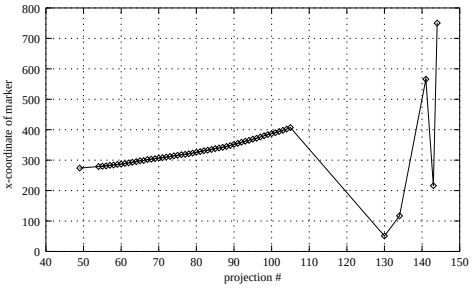

(a) Selected markers.

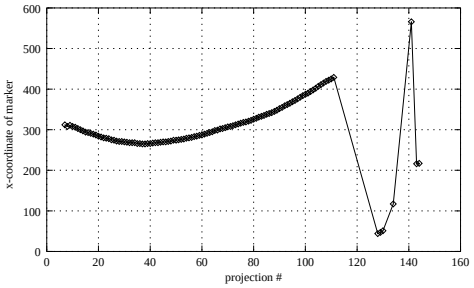

(b) Markers after first tracing step.

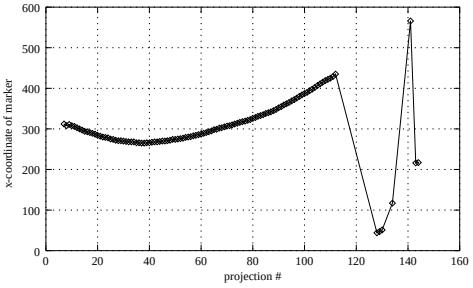

(c) Markers after second tracing step.

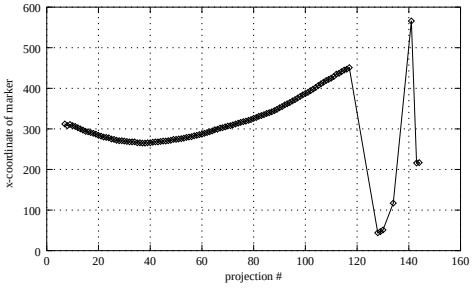

(d) Markers after third tracing step.

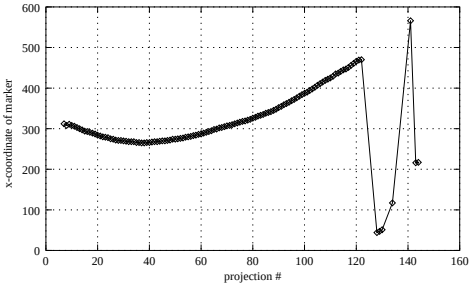

(e) Markers after forth tracing step.

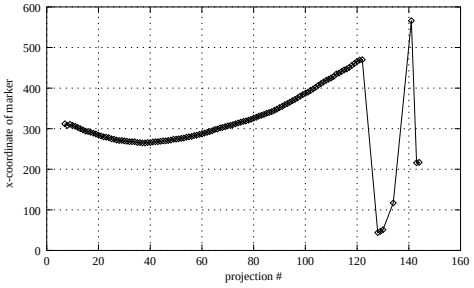

(f) Markers after fifth tracing step.

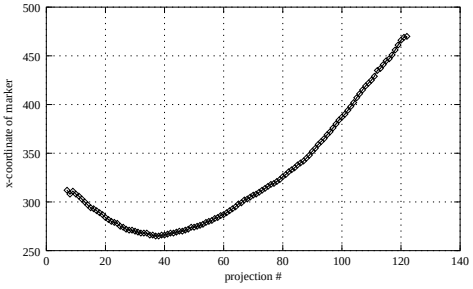

(g) Finally indexed markers.

Figure B.12: Cluster 11.

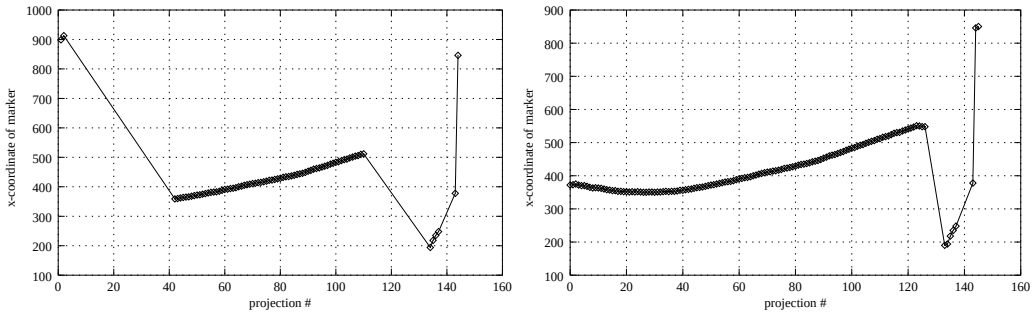

(a) Selected markers.

(b) Markers after first tracing step.

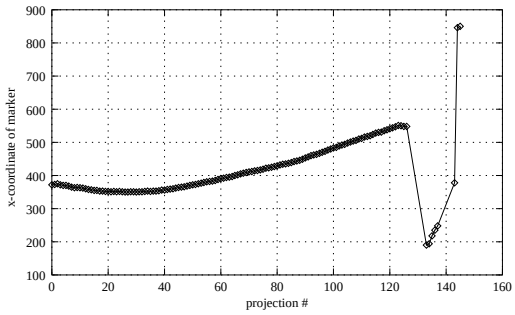

(c) Markers after second tracing step.

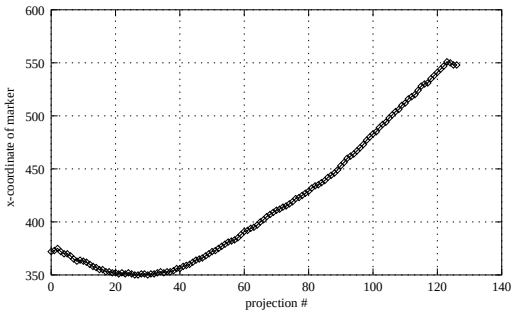

(d) Finally indexed markers.

Figure B.13: Cluster 12.

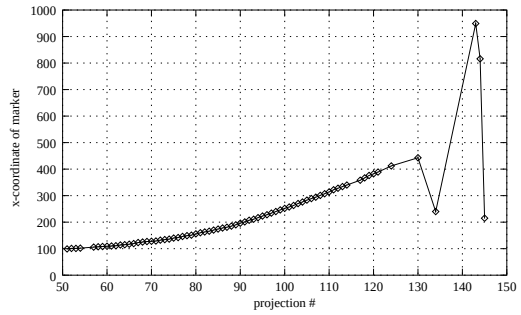

(a) Selected markers.

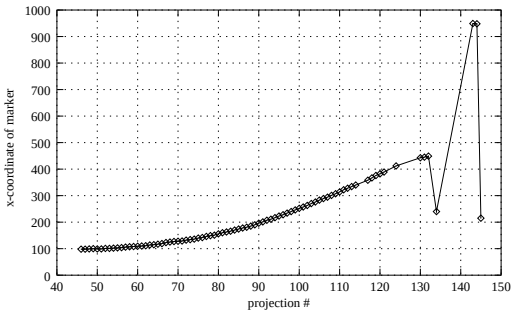

(b) Markers after first tracing step.

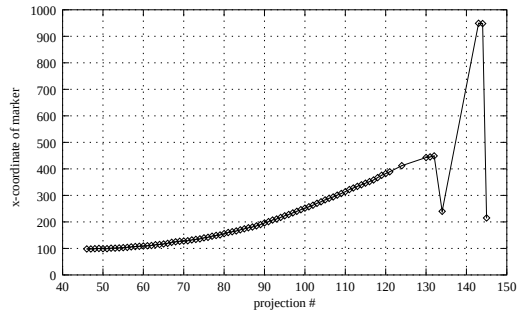

(c) Markers after second tracing step.

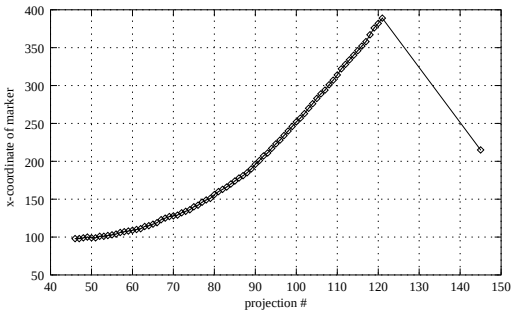

(d) Finally indexed markers.

Figure B.14: Cluster 13.

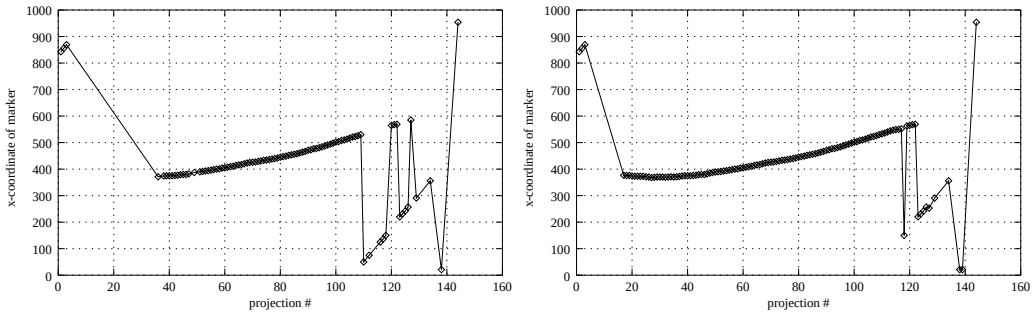

(a) Selected markers.

(b) Markers after first tracing step.

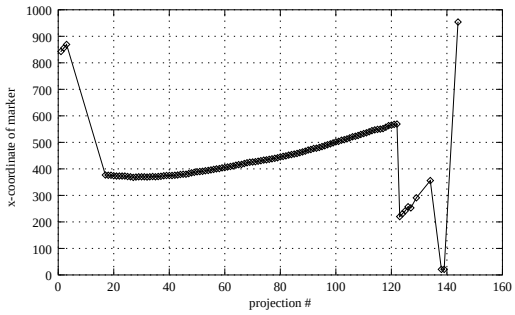

(c) Markers after second tracing step.

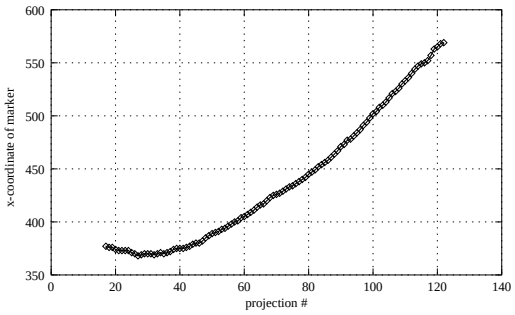

(d) Finally indexed markers.

Figure B.15: Cluster 14.

Acknowledgements

I would like to thank all those who contributed to the success of this work. It would have been impossible without the cooperation of a large amount of people.

I would like to thank Prof. Dr. Herbst for being a referee of this thesis.

Foremost, on the side of the research laboratories, I thank Dr. Thomas Köhler who defined this work and who was always ready for discussion and thus supported the proceeding of my work.

I wish to thank Dr. Thomas Netsch from the Digital Imaging group who developed the feature detection algorithm and thus detected the features tracked by the presented algorithm.

Furthermore, my thank goes to my student colleagues and all the staff of the Philips Research laboratories for a friendly atmosphere at work, in particular: Christof Baltes and Robert Manzke.

Last but not least, I would like to thank Robert Brown for having a closer look on the English language.

I hereby declare that this submission is my own work and that, to the best of my knowledge and belief, it contains no material previously published or written by another person nor material which to a substantial extent has been accepted for the award of any other degree or diploma of a university of applied sciences or other institute of higher learning, except where due acknowledgement has been made in the text.

Hamburg, November 10th 2000 Kerstin Stockmeier